Spring 2020

Crystalline architecture and stratigraphy of coral skeletal density banding: a geobiological record of changing coral reef ecology

Kyle Fouke
Bucknell University, kwf005@bucknell.edu

CRYSTALLINE ARCHITECTURE AND STRATIGRAPHY OF CORAL SKELETAL DENSITY BANDING: A GEOBIOLOGICAL RECORD OF CHANGING CORAL REEF ECOLOGY

by

Kyle W. Fouke

A Thesis

Presented to the Faculty of Bucknell University

In Partial Fulfillment of the Requirements for the Degree of Bachelors of Science
With Honors in Geology

April 9, 2020

Approved by:

Adviser: 

Professor Jeffrey M. Trop

Second Evaluator: 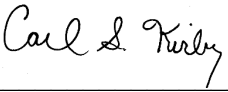

Professor Carl Kirby

ACKNOWLEDGEMENTS

I would first like to thank my advisor Professor Jeffrey Trop for his guidance and his commitment to advising and teaching me in the classroom and the field throughout my four years at Bucknell. It has allowed me to successfully complete this thesis project and leave Bucknell a confident geologist. I deeply appreciate his willingness to allow me to conduct a research project on coral skeletons. Thank you to the faculty and staff in the Bucknell Department of Geology and Environmental Geosciences. I would especially like to thank Carilee Dill and Brad Jordan as both of them were sturdy resources and supporters for me and work hard every day to make the department run smoothly and effectively. I deeply appreciate Professor Carl Kirby being the second reader for my senior thesis and sharing his expertise about geochemistry for the project and in his classroom. I am very grateful to Professor Mary Beth Gray for letting me be her Teaching Assistant for two semesters to help me become a better teacher in the geosciences. I am grateful for the hard work of Professor Trop, Professor Chris Daniel, Professor Gray, and Professor Ellen Chamberlin in developing multiple spring break trips to the southwest to deepen my understanding of the Earth, become comfortable in geologic field mappings, and giving me the opportunity to make truly meaningful relationships with the faculty and other students. I am very grateful to Professor Kelly Bickel who served as the third reader on my senior thesis honors thesis committee.

This project could not have been completed without the help of excellent scientists and researchers outside of the Bucknell campus. Mark Vermeij and the CARMABI staff on Curaçao for their help in my field collection and providing adequate lab space and

dormitories to conduct intense field collection of the coral heads. I also wish to express my sincere thanks and appreciation to Dr. Mayandi Sivaguru (Shiv), Associate Director of the Microscopy and Imaging Core in the Carle R. Woese Institute for Genomic Biology at the University of Illinois Urbana-Champaign. From the bottom of my heart, I deeply appreciate the tremendous effort and support he puts forth for my senior thesis and scientific career. Furthermore, I would like to recognize Dr. Peter Yau who has helped me start my scientific career during the summers I spent in his lab where his mentoring left a wonderful impact on me that has helped me to this day and into the future.

Lastly, I could not have completed this project without the incredible people that I have met at Bucknell and my family. Thank you to all the Geopalz who took over room 105 in the basement of O'Leary with me over my four years at Bucknell. Everyone truly made that computer lab feel like home and I will always look back on the wonderful times spent with the geology students. Shout out to Ali, Sam, Sam, and Matylda that came to Bucknell with a declared geology major with me. I will deeply appreciate Evan Filion and Matylda Zaklicki who were the other Sedheads who endured the grind and late nights in O'Leary and on Zoom in completing a senior thesis with me. Our respective senior thesis projects brought us closer together and I wouldn't want any other people by my side in this endeavor. Additionally, I am very grateful for Matt, John, Andrew, and Evan who have become my brothers after countless of hours of laughter, rain, yelling, joking, and trail singing in the Adirondacks and other wildernesses around the United States. These guys helped me stay sane and pulled me out of continuous work to have some fun during my senior thesis. I am also extremely grateful to Ellie Covert for loving me and continually

making me be the best person that I can be. She made sure that I got adequate sleep and stayed healthy through the stressful moments and always knew how to cheer me up through the sad times. She was there for me when I needed her and I would not want to share the life-changing experiences and moments that I had with her at Bucknell with anyone else. Thank you, Ellie from the bottom of my heart. And I couldn't finish this project with the support of my dad, mom, and my sisters Kaitlyn and Courtney. My parents give me unconditional love and support every day that I am truly grateful for as they push me to try my best every day and have shown me the world. Thank you, Dad for being the professor Dad that any kid would want. Thank you, Mom for the passionate support and amazing home cooking as I had to shift to online classes. I am grateful for the goofballs that I call my sisters who always know how to make me laugh and support me through good ol' fashion family love.

This research was supported by grants from the Geological Society of America and the Evolving Earth Foundation. *Orbicella annularis* specimens were collected under permits issued from the Caribbean Research and Management of Biodiversity (CARMABI) laboratory, and the Curaçao Ministry of the Health, Environment, and Nature. In addition, I sincerely appreciate receiving the PK2006 *O. annularis* head sample from the Fouke Research Group at the Carl. R. Woese Institute for Genomic Biology at the University of Illinois Urbana-Champaign.

TABLE OF CONTENTS

LIST OF FIGURES

ABSTRACT

Coral skeletal density banding (CSDB), composed of alternating high density band (HDB) and low density band (LDB) layers that comprise the $CaCO_3$ (*aragonite*) skeleton of scleractinian corals, are used as chronometers for global paleoclimatic reconstructions of sea surface temperature (SST). Scleractinian coral skeletons have been intensively studied for centuries with detail analysis of the macro- and microscale skeletal structure to establish taxonomic and evolutionary relationships of coral species, mechanisms of biomineralization, and seafloor physical, chemical and biological alteration (diagenesis) of the skeleton. This study is the first to determine the crystalline architecture of HDBs and CSDB stratigraphic sequences in original unaltered scleractinian coral skeletons and how this might impact CSDB-derived SST reconstructions. High-resolution optical microscopy, microcomputed tomography (microCT) scans, and x-radiography analyses are presented of CSDB in *Orbicella annularis* collected in 2006 and 2019 from the fringing reefs at Playa Kalki (PK) and Snake Bay (SB) on the southern Caribbean island of Curaçao. Results indicate that HDB layers are formed by the thickening of skeletal components (*thecal walls*, *costae walls*, and *exothecal dissepiments*) outside the margin of individual skeletal cups (*corallites*) that house living coral polyps. Conversely, skeletal elements within each corallite (*septal walls* and *endothecal dissepiments*) do not exhibit crystalline thickening. In addition, minor seafloor physical, chemical and biological alteration (diagenesis) is observed in both HDBs and LDBs. CSDB stratigraphic sequences exhibit down lap, condensed sections, and cross-cutting relationships that represent changes in coral ecology and growth history. Multiple HDB-LDB couplets were observed to be <5 mm in thickness,

which combined with previously recorded *O. annularis* growth rates, indicate that these couplets represent less than one year of skeletal growth and do not reflect annual changes in SST. The PK2006 head records a hiatus event where coral growth shifted laterally, exposed part of the outermost coral skeletal surface to fungal borings and encrusting organisms, and was then later overgrown by the same coral colony. No specific HDB, LDB, or other stratigraphic intervals could be successfully correlated using microCT and x-radiograph line profiles between the PK2006, PK2019 and SB2019 coral heads. These results suggest that CSDB formation is strongly ecologically influenced by the host coral, symbiotic zooxanthellae, and resident microorganisms (collectively called the *coral holobiont*). Therefore, the influence of these biotic processes needs to be factored into CSDB-derived SST paleothermometry to create accurate predictions of future climate change.

INTRODUCTION

Scleractinian "stony" corals, which form hard calcium carbonate ($CaCO_3$) skeletons in the mineralogical form of aragonite, have been intensively studied for centuries from a wide variety of perspectives. Key examples include: (1) overall macroscale form and growth symmetry (e.g. Haeckel 1873); (2) macroscale taxonomic identification and allometric analyses of whole coral skeletons (*heads* or *coralla*) in order to understand modern and ancient reef ecology and identify marine carbonate depositional facies models (e.g., Wells, 1954; Goreau 1963; Wilson 1975; Bak and Luckhurst 1980; Van Duyl 1985; Flügel 2004; Klaus et al. 2015; Dornela et al. 2017); (3) meso- and

microscale analyses of skeletal structure and post-depositional physical, chemical and biological diagenetic alteration (*diagenesis*) for use in reconstructions of paleoclimate (e.g., Barnes and Lough, 1993; Hendy et al. 2007; Northdurft and Webb 2007; Sivaguru et al. 2019); (4) micro- and nanoscale structural analyses for use in determining numerical taxonomy and reconstructing evolutionary relationships (e.g. Stolarski and Roniewicz 2001; Budd et al. 2012; Kitano et al. 2014); (5) micro- and nanoscale analyses to determine mechanisms of biomineralization (e.g. Cuif et al. 1998; Cohen and McConnaughy 2000; Allemand et al. 2011; Frankowiak et al. 2016); and (6) microscale geobiochemical and structural analyses for use as human and animal bone grafts (Demers et al. 2002; Fessenden 2014).

Especially important and timely among these studies is the analysis of the structure and geochemistry of coral skeletons to reconstruct ancient sea surface temperature (SST). The record-breaking warm period of 2015 through 2020 continues the dramatic increase of average Earth temperatures (Blunden et al. 2017; NOAA-NCDC 2020). Accurate predictions of future global warming are vital to guide societal planning to survive the environmental impacts of sea level rise, ocean acidification, drought, disease and fire (Hoegh-Guldburg et al. 2007; Barkley et al. 2015; IPCC 2018). The accuracy of climate change forecasts is determined by comparing instrumental measurements to past temperature changes recorded by environmental "proxy" records (IPCC 2018). Especially valuable are seasonal changes in SST recorded by coral skeletal density banding (CSDB) traditionally detected with standard x-radiography and most recently with microcomputed tomography (microCT). CSDB sequences, which are composed of alternating high-density

bands (HDBs, warm summer-fall SST season) and low-density bands (LDBs, cool winter-spring SST season), are thought to be the only proxy to record high-frequency seasonal changes in ocean circulation and climate, such as the El Niño–Southern Oscillation (Alibert et al. 1997; Cruz-Piñón et al. 2003; Alpert et al. 2016; IPCC 2018).

The zooxenthellate coral *Orbicella annularis* (previously named *Montastraea annularis*, Budd et al. 2012) is commonly used for Caribbean Sea SST paleothermometry because it forms large (<2 m-diameter) columnar to hemispherical heads that exhibit well-developed CSDB as detected with x-radiography (Carricart-Ganivet 2004; Worum et al. 2007). *O. annularis* heads are either drilled for skeletal cores, or whole heads are collected, to reconstruct decades-long SST from vertical transects of $\delta^{18}O$ and Sr/Ca skeletal chemistry preserved within CSDB layering (Van Veghel and Bosscher 1995; Carricart-Ganivet 2004). The fidelity of these CSDB-derived SST reconstructions is evaluated via direct comparison with instrument measurements of SST collected over the last 125 years on tropical reefs distributed around the world. While generally accurate, these reports have also identified specific CSDB intervals that underestimate instrument-based SST by as much as 9°C (Sivaguru et al. 2019). Improved interpretation and correction of these anomalous CSDB-derived SST intervals requires a systematic understanding of CSDB formation that has yet to be established.

For example, in addition to seasonal changes in SST, the formation of HDBs and LDBs are known to be strongly influenced by coupled coral and zooxanthellae physiological responses to other abiotic ecological parameters such as climate, lunar cycles and solar radiation (Barnes and Lough 1993; DeCarlo and Cohen 2017). Another

influential factor is that *O. annularis* skeletons undergo physical, chemical and biological alteration (*diagenesis*) in the marine environment where they originally grew (Quinn and Taylor 2006; Nothdurft et al. 2007; McGreggor et al. 2008; Sayani et al. 2011; Sivaguru et al. 2019). As a result, the thickness, lateral continuity, intensity and overall layering patterns (*stratigraphic sequence*) of CSDB are all vulnerable to seafloor diagenesis. A recent study of *Porites* on the Great Barrier Reef has made quantitative correction factors for these diagenetic effects on CSDB-derived SST, showing that as little as 5% diagenetic marine aragonite cement can cause an ~1°C error in reconstructed SST (Sivaguru et al. 2019).

Several untested assumptions are made in previous studies using CSDB to reconstruct paleoclimatic estimates of SST (e.g., Lough and Barnes 1989; De'ath et al. 2009; Alpert et al. 2016). This includes CSDB sequences of HDBs and LDBs have been assumed to represent continuous, undisrupted growth of the coral skeleton (e.g. Knuston et al. 1972; Lough and Barnes 1989; Cruz-Piñón et al. 2003). In addition, it has been assumed that the most pristine and continuous skeleton is located within the central portion of coral heads due to bioerosion observed on the margins (e.g. Hendy et al. 2007; Northdurft and Webb 2007; Alpert et al. 2016). Studies have largely ignored the margins of the coral skeletons assuming that they do not hold useful information. Furthermore, each HDB-LDB couplet has been assumed to represent one-year of growth in response to a complete seasonal cycle (e.g. Knutson et al, 1972; Barnes and Lough 1989; Sayani et al. 2011). CSDB can to be used as a reliable chronometer, like tree rings, and provide absolute dating for isotopic analyses given these assumptions are valid.

This present study builds directly upon this extensive literature base and combines strategic spatial and temporal field sampling with high-resolution microscopy, microCT, and x-radiograph analyses to determine the crystalline architecture and stratigraphy of CSDB sequences of original *O. annularis* skeletons. Detailed analyses will be used to determine the validation of the core assumptions in CSDB-derived SST models. Evidence will be presented that CSDB is strongly ecologically influenced by the host coral, symbiotic zooxanthellae, and resident microorganisms (collectively called the *coral holobiont*). Therefore, these biotic processes should be recognized and included when evaluating CSDB-derived SST as a means to test future modelling of global climate change.

MATERIALS AND METHODS

Geobiological Setting of Curaçao

The southern Caribbean island of Curaçao (Fig. 1), which recently became independent from the Netherlands Antilles, lies 65 km north of Venezuela within the east-west trending Aruba-La Blanquilla archipelago. The 45 km-long southwestern leeward coast of Curaçao (Fig. 1A) contains a continuous modern fringing coral reef tract that has experienced rapid Neogene uplift (along the contact of the Caribbean and South American crustal plates) to form a well-preserved succession of Miocene through Holocene fossilized coral reef limestone deposits called the Seroe Domi Formation and Quaternary Reef Terraces (Fouke et al. 1996). Mean annual SST on Curaçao varies ~3°C annually, ranging

from a minimum of ~26°C in late January to a maximum of ~29°C in early September, with a mean annual temperature of 27.5°C ± 0.5°C (NOAA 2020).

The modern fringing reef ecosystem of Curaçao provides an especially well-suited natural laboratory for the present study of CSDB. This is because: (1) the coral reefs on Curaçao have been well-studied and monitored for nearly 70 years, during which time an extensive literature base has been established of their modern and ancient composition, structure and biodiversity (e.g., van Duyl 1985; van Veghel 1994); (2) the entire Curaçao coral reef tract has been a protected underwater national park since 1955 (van Duyl 1985; Bak and Luckhurst 1980); (3) the shallow marine shelves surrounding Curaçao are extremely narrow due to the rapid tectonic uplift of the island (Fouke et al. 1996), thus the reef crest and shelf break environments of the fringing coral reef ecosystems are only 200m to 500m from shore (van Veghel 1994; Bak and Luckhurst 1980)(Fig. 1B); (4) as a result, virtually the entire Curaçao fringing reef system is accessible via “easy entrance” shore-based SCUBA dives and thus boat diving is not required; and (5) the Caribbean Research and Management of Biodiversity (CARMABI) laboratory; formerly called the Caribbean Marine Biological Institute has been in existence since 1955 and has provided the research base for the present study (Debrot and Bak 2019).

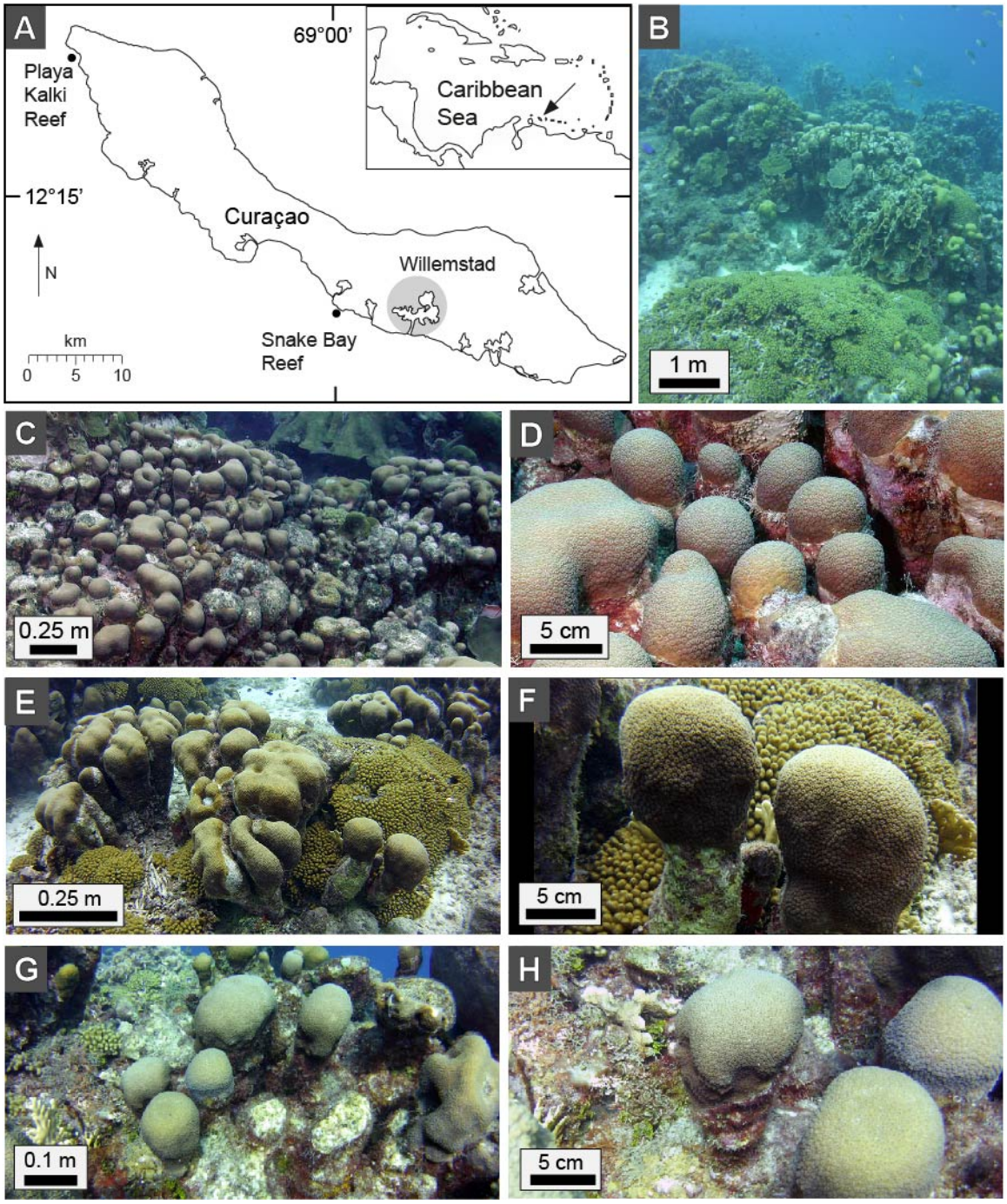

Figure 1. Geobiological context of *Orbicella annularis*. (**A**) Map of Curaçao with insert showing location (arrow) of the island in the southern Caribbean Sea. Playa Kalki and Snake Bay sample sites are shown, as well as the capital city of Willemstad. (**B**) Underwater field photograph of the 10 m water depth shelf break at Playa Kalki. Left side

of the photograph is at 8 m water depth where the PK2006 and PK2019 heads of *Orbicella annularis* were collected. Water depth increases to 15 m at the right side of the photograph. (**C-D**), *O. annularis* heads at Playa Kalki in August 2019 (**E-F**), and *O. annularis* heads at Snake Bay in August 2019 (**G-H**).

Choice of *O. annularis* as a Model Organism for Studies of CSDB

O. annularis was chosen for this study because it exhibits distinct well-developed CSDB that has been well-documented and it is the most commonly used coral to reconstruct sea surface temperature (SST) in the Caribbean Region (Carricart-Ganivet 2004; Worum et al. 2007; Carricart-Ganivet 2007; Carricart-Ganivet et al. 2012). *O. annularis* is also the most volumetrically important cornerstone framework builder of both modern and ancient coral reefs throughout the Caribbean Sea to record a robust record of SST (van Veghel, 1994; Bak and Luckhurst 1980; Carricart-Ganivet 2004). As a result, the ecology, physiology and evolutionary relationships of *O. annularis* have been previously well-studied (Bak and Luckhurst 1980; Salih et al. 2000; Knowlton and Budd 2001). *O. annularis* is also known to consistently grow within a very narrow bathymetric range of $\leq$10 m WD (van Duhyl 1985; Fukami et al. 2004). In addition, the genome of the closely related species *O. faveolata* has been completed (Schwartz et al. 2008; Desalvo et al. 2008). This will permit future CSDB studies of *O. annularis* to be correlated with coral genomic structure and composition under controlled experimental conditions.

O. annularis, *O. faveolata*, and *Monastraea franksi* comprise the *Orbicella-Montastraea* species complex (Knowlton and Budd 2001). These three species were originally considered ecophenotypes of one species, *O. annularis*, until recent studies of molecular phylogeny, behavior, microstructure of the skeleton, geochemistry, and growth rate, that corresponded with the different colony morphologies (e.g., Knowlton et al. 1992, 1997; Wallace and Willis 1994; Veron 2000; Budd et al. 2012).

Sample Sites and Field Collections

The sampling strategy for the present study was to directly compare the crystalline architecture and stratigraphy of *O. annularis* CSDB at the same water depth (WD) in two different geologically and environmentally equivalent sites in 2006 and 2019 across the leeward reef tract of Curaçao (Fig. 1). Sampling for the present study was first conducted in March 2006 by the Research Group of Professor Bruce W. Fouke at the University of Illinois Urbana-Champaign, when a single 8 cm by 11 cm head of *O. annularis* was collected at 8 m WD in the back reef depositional facies tract of Playa Kalki (PK; 12°22'29"N, 69°09'29"W; Fig. 1C, D; Wilson 1975; Flügel 2004). An additional round of field collection by myself took place in August 2019, when two more small heads of *O. annularis* were collected at 8 m WD in the back reef depositional facies of both Playa Kalki (11 cm by 22 cm; Fig. 1E, F) and Snake Bay (SB; 11 cm by 18 cm; 12°08'19"N, 68°59'52"W; Fig. 1G, H). The 2006 and 2019 samples of *O. annularis* colonies at Playa Kalki were collected from within a few meters of each other at 8 m WD just landward of the shelf break in the back reef depositional facies.

Playa Kalki and Snake Bay were chosen for this study because their marine ecosystems have been quantitatively shown to be bathed in fresh minimally-polluted seawater (Frias- Lopez et al. 2002; Klaus et al. 2007). A unidirectional SE-NW offshore current moves along the leeward coast of Curaçao and the sewage effluent and storm runoff from the densely populated municipal, industrial and military seaport of Willemstad that surrounds St. Annabaai (Fig. 1A). These pollutants directly impact and reduce photosynthetically active radiation (PAR) offshore from Willemstad and uptake of sewage-

derived compounds by *O. annularis* is demonstrated by the $\delta^{15}N$ of the tissue (Klaus et al. 2007). As the current flows to the northwest along the length of the island, the marine environment exhibits: (1) systematic decreases in the extent of seawater pollution; (2) changes in coral mucus composition; (3) alteration in the composition of bacterial communities inhabiting the coral tissues; and (4) the photosynthetic activity of the endosymbiotic zooxanthellae (Klaus et al. 2007). By the time that currents reach Snake Bay and Playa Kalki, the seawater has been mixed and diluted and returned to its original normal marine and minimally-impacted biogeochemical composition with no further influence on PAR and organic matter uptake (Klaus et al. 2007).

Living *O. annularis* heads have been strategically sampled for this study within the context of the marine carbonate depositional facies tracts in which they grow. This serves to ensure environmental consistency between individual reef sample sites and will allow the results of the present study to be more accurately applied in future research on ancient coral reef limestone deposits on Curaçao and throughout the Caribbean Basin (Fouke et al. 1996). Coral reef depositional facies are defined as distinct sedimentary units formed on the seafloor as a result of the combined physical, chemical and biological processes present in the marine environment at the time of deposition (Wilson 1975). The primary physiographic feature on a fringing coral reef is the shelf break, where a dramatic change in the slope of the reef occurs as the seafloor plunges downward toward the deep ocean basin (Wilson 1975). The shelf break defines the boundary between the landward back reef environment and the seaward fore reef slope, each of which experiences distinct environmental parameters (Wilson 1975; Flügel 2004). In the present study, *O. annularis*

was consistently and systematically collected in both 2006 and 2019 in the back reef depositional facies at the 8 m WD just landward of the shelf break (Fig. 1B).

SCUBA Collection of *O. annularis*

Fieldwork for this project was based out of the CARMABI on Curaçao. The three *O. annularis* coral heads for this study were collected by myself with permission of the Curaçao Ministry of the Health, Environment, and Nature, as well as CARMABI. Collections of small healthy heads of *O. annularis* (Fig. 1) were made in March 2006 at Playa Kalki and August 2019 at Playa Klaki and Snake Bay (Fig. 1A). Heads were collected using a clean Estwing geology hammer and chisel, held with gloved hands, while on standard compressed-air SCUBA dives at 8 m WD. Only the uppermost growing end of *O. annularis* columns were collected, to ensure minimal impact on the rest of the living colony (Fig. 1). Absolute dating of these types of modern coral skeletons is challenging. Therefore, the August 2019 samples from Playa Kalki (PK) and Snake Bay (SB) were specifically chosen to be approximately double the length of the March 2006 sample from Playa Kalki, in order to attain temporal stratigraphic overlap of CSDB comprising the three heads for correlation of the 2016 age of the uppermost growth surface of PK2006. Immediately upon collection at depth, each head was gently placed in a net bag and brought to the surface. Each head was then placed in a seawater-filled clean plastic bucket and transported back to the CARMABI laboratory, where the samples were then submerged in a clean plastic bucket containing a dilute solution of 2.5% sodium hypochlorite. This removed coral tissue and organic matter trapped within the matrix of each coral head, while

not being strong enough to dissolve the skeletal aragonite (Love and Woronow 1991). Within two days after sampling, each head sample was placed in clean bubble-wrap and carefully inserted into rigid PVC tubing for safe damage-proof shipping to the University of Illinois at Urbana-Champaign. Each coral head was placed in a clean plastic bucket containing a dilute solution of 2.5% sodium hypochlorite for an additional month of tissue and organic matter removal.

MicroCT and X-Ray Analyses

The PK2006, PK2019, and SB2019 *O. annularis* heads were brought to the University of Texas Computed Tomography (UTCT) facility where the facility staff imaged of the entire heads at 63 μm-resolution on a microcomputed tomography (microCT) imaging system (North Star Imaging, Feinfocus 225 kV; Fig. 2). After the microCT scans were acquired, I analyzed the resulting three-dimensional (3D) x-ray data sets at the Microscopy and Imaging Core Facility of the Carl R. Woese Institute for Genomic Biology on the University of Illinois at Urbana-Champaign campus. The several thousand microCT images collected from each *O. annularis* head were compressed and converted into a maximum intensity 3D volume projection that represents a 5 mm virtual skeleton slice. Slices through the virtual 3D projections permitted determination of the optimal orientation in which to physically cut the skeletons for the most complete and continuous CSDB section. In turn, this permitted optimal positioning for cutting slices for x-radiography analyses and thin section billets.

Each coral head was then cut into 5 mm-thick vertical slices using a clean diamond tile saw. The coral skeleton slices were taken to the University of Illinois at Urbana-Champaign Veterinary School of Medicine to be further imaged using a standard x-radiograph system (Siemens Model #10092624, 70 kV; Fig. 3). All x-radiograph and microCT images presented in this study, unless otherwise indicated, are direct CSDB, where darker layers are low-density bands (LDBs) and lighter layers are high-density bands (HDBs).

Quantitative Analyses of CSDB in MicroCT and X-Ray

All image compression, averaging, gray scale corrections, and line profile analyses, were conducted using NIH Image J software (https://imagej.nih.gov/ij/). I completed quantitative line profile image analyses to quantify CSDB layering patterns and potentially establish correlations between the 2006 and 2019 coral heads. The line profiles could help in identifying HDBs and LDBs that are not easily seen with the naked eye. This quantitative data analysis approach may reveal more realistic correlations between the heads. Averaged MicroCT and raw XRD images were converted to TIFF files at both 8-bit and 16-bit gray scales for comparative visualization. Line transects were created to establish complete bottom-to-top (i.e. older-to-younger) CSDB stratigraphic sequences in all heads for both MicroCT and XRD. Line widths were adjusted to a width of 200 pixels on the 2006 coral head and 500 pixels on the 2019 coral heads. The smaller line width in the 2006 coral head was chosen as the 2006 head is smaller than the two 2019 heads. All line widths were set to reduce natural CSDB curvature in the line profiles that would otherwise increase noise

in the analyses. Along each transect, a line profile of the gray scale intensity was plotted where higher gray scale valves represent white/light gray areas and low gray scale values represent dark gray/black regions. Therefore, high intensity peaks represent HDBs and low intensity troughs between high intensity peaks represent LDBs.

Thin Sectioning and Optical Microscopy

Standard size thin section billets were cut from the PK2006, PK2019, and SB2019 coral heads in locations indicated by the white boxes shown on the x-radiograph images in Figure 3A. Each billet was prepared as an ultrathin 25 μm-thick thin section by Wagner Petrographic (Linden, Utah), where it was impregnated with blue-dyed epoxy, affixed to a standard-sized petrographic glass slide, trimmed, doubly polished and mounted with no cover slip. All optical microscopy was conducted on instruments housed in the Microscopy and Imaging Core Facility of the Carl R. Woese Institute for Genomic Biology at the University of Illinois Urbana-Champaign. Dr. Mayandi Sivaguru helped me virtually control and run the microscopes at Bucknell University to complete microscopic analyses myself. Two optical microscopic techniques were utilized in this study to investigate the crystalline composition and structure of CSDB in thin section, which included bright field (BF), polarization (POL), and phase-contrast (PC) techniques (further details are presented in Sivaguru et. al (2019)). These optical analyses were conducted at a resolution of ~250nm on a Zeiss Axiovert 200M, as well as on a Zeiss Axioscan Z1 whole slide scanning system with 20x, Plan Apochromat 0.8 NA and 50x Plan Neofluar 0.95 NA POL objectives (for both BF and POL). Digital thin section transparencies of all modalities were overlaid at

~50% opacity on x-radiograph images for each whole thin section to determine the precise position of HDBs and LDBs. This permitted optical microscopy to be completed within the precise spatial distribution of the CSDB stratigraphy shown only in the x-radiographs.

Image Processing

MicroCT and x-radiograph digital images were converted to 8-bit gray scale to analyze and potentially correlate CSDB stratigraphic sequences among the three coral heads collected. All optical microscopy images were processed using Zeiss Zen Blue software on workstations in the Microscopy and Imaging Core Facility of the Carl R. Woese Institute for Genomic Biology at the University of Illinois Urbana-Champaign. Thin section scans and images were adjusted after all the procedures outlined above were completed. Red, green, and blue (RGB) curves were adjusted and presented as linear or with a gamma adjustment of 0.4-0.5, min/max, best mode or manually adjusted in the display properties window in the Zeiss Zen software for representative brightness, contrast and clarity. Final images were cropped, aligned, and resized where necessary. Image adjustments were performed in Adobe Photoshop and Adobe Illustrator (Adobe systems, San Jose, CA). In addition, the 3D virtual visualization of microCT images and creation of 3D images was completed using Imaris 3D Visualization software (Bitplane, Zurich, Switzerland). I completed all image processing by myself in this study. Dr. Sivaguru taught me the techniques and programs necessary for the image processing.

RESULTS

O. annularis heads grow either as massive hemispherical colonies or as multiple columns (Weil and Knowlton, 1994; Humann and DeLoach 2001). Heads PK2006, PK2019, and SB2019 were collected from the 12 to 22 cm uppermost living top of *O. annularis* columns (Fig. 1C-H). The living tissues are light brown due to the pigments of their symbiotic photosynthetic zooxanthellae (Figs. 1C-H), which combined with the host coral and its multiple microorganisms are called the coral holobiont (Rohwer et al. 2001). Recent research has revealed an extensive coral microbiome that includes dinoflagellates, viruses, fungi, archaea, and bacteria that influence coral biological processes within the tissue and the coral skeleton (Van Oppen and Blackall 2019; Ricci et al. 2019). These multiple microorganisms have yet to be studied in the context of coral skeletons or CSDB but may influence these factors. The lower regions of each column below the living tissue are composed of exposed coral skeleton that is encrusted with coralline algae, bryozoans, sponges, and serpulid tube worms that bore into the skeleton (Fig. 1H).

CSDB Stratigraphy

MicroCT 3D volume projections, microCT virtual cross-sections, and x-radiograph cross-sections of all three *O. annularis* heads are shown in Figures 2 and 3. These exhibit high-frequency hemispherical HDB and LDB layering that reflects upward coral growth vertically and laterally at the top of each column. This creates distinct continuous concave-down stratigraphic sequences across the entire coral head (Figs. 2, 3, 4). These CSDB layering patterns include multiple examples of stratigraphic downlap, onlap, layers

becoming thinner, condensed, and pinching out laterally (*condensed section*), and cross-cutting relationships, all of which are commonly cross-cut by bioerosional borings (Fig. 4). In addition, an HDB event surface in PK2006 exhibits multiple events of skeletal growth, fungal borings, seafloor dissolution and encrustation by serpulid tube worms, coralline algae and bryozoans (Fig. 5). This specific HDB event surface is laterally continuous with an HDB created by original skeletal thickening (Fig. 5).

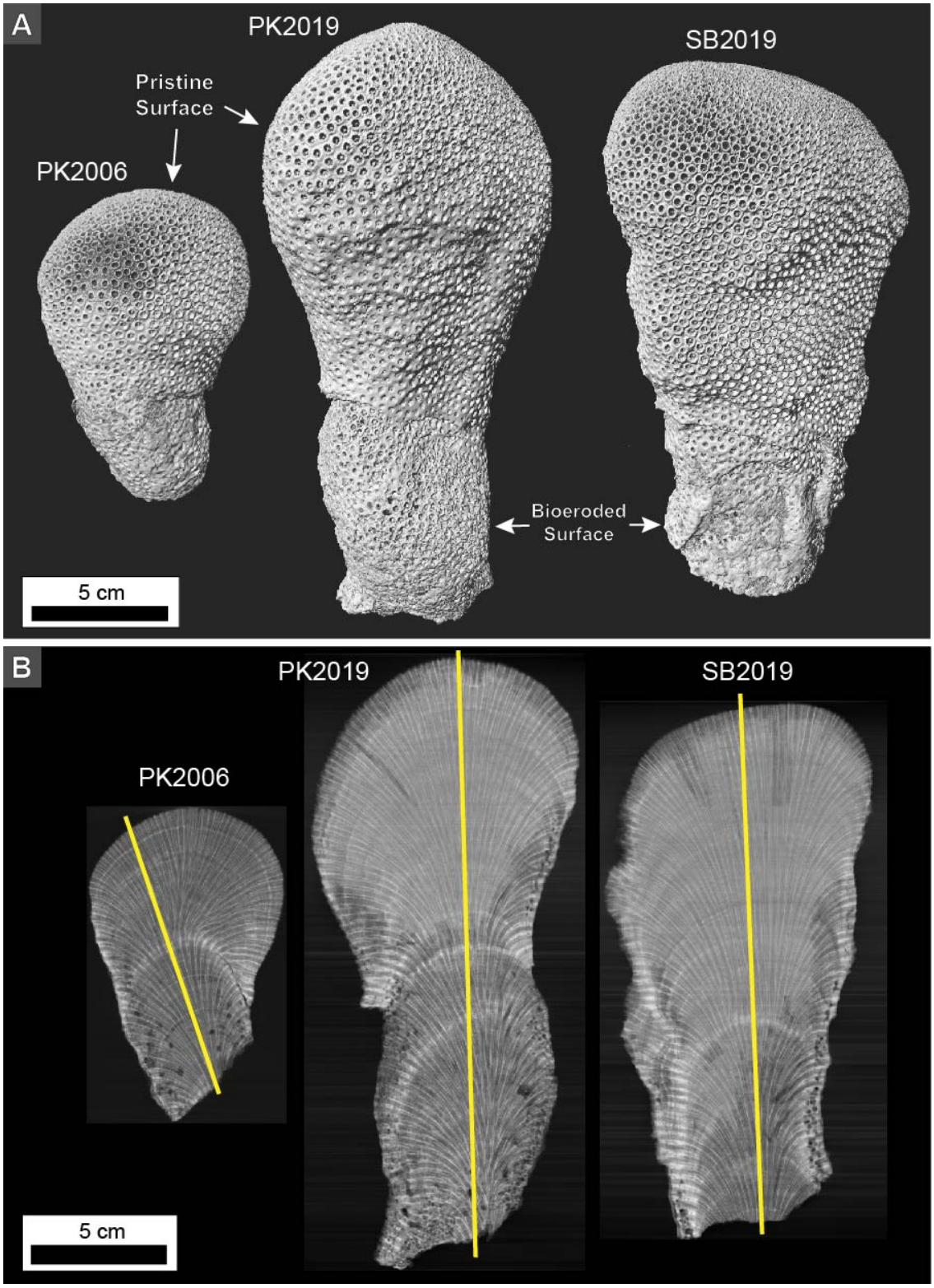
A
PK2019
SB2019
Pristine
Surface
PK2006
Bioeroded
Surface
5 cm
B
PK2019
SB2019
PK2006
5 cm

Figure 2. MicroCT scans of *O. annularis* heads. (**A**) Maximum intensity 3D volume projections. The upper two-thirds of each head are pristine surfaces composed of corallites that were living at the time of sampling. The lower third of each head is composed of encrusted and bioeroded surfaces that were not living at the time of sampling. (**B**) Virtual 5 mm-thick vertical slices of the 3D volume projections in **A**. Coral skeletal density banding (CSDB) is shown as alternating high-density bands (HDBs, light gray to white layers) and low-density bands (LDBs, dark gray to black layers). Yellow lines indicate location and orientation of line profile analyses presented in Figures 4 and 5. Note that there was not sufficient time for the 2.5% sodium hypochlorite solution to fully remove the tissue and organic matter from within each head. The remaining organic matter inside the skeleton caused the MicroCT scans to exhibit a diffuse blurred gray character that partially masked the CSDB within those areas.

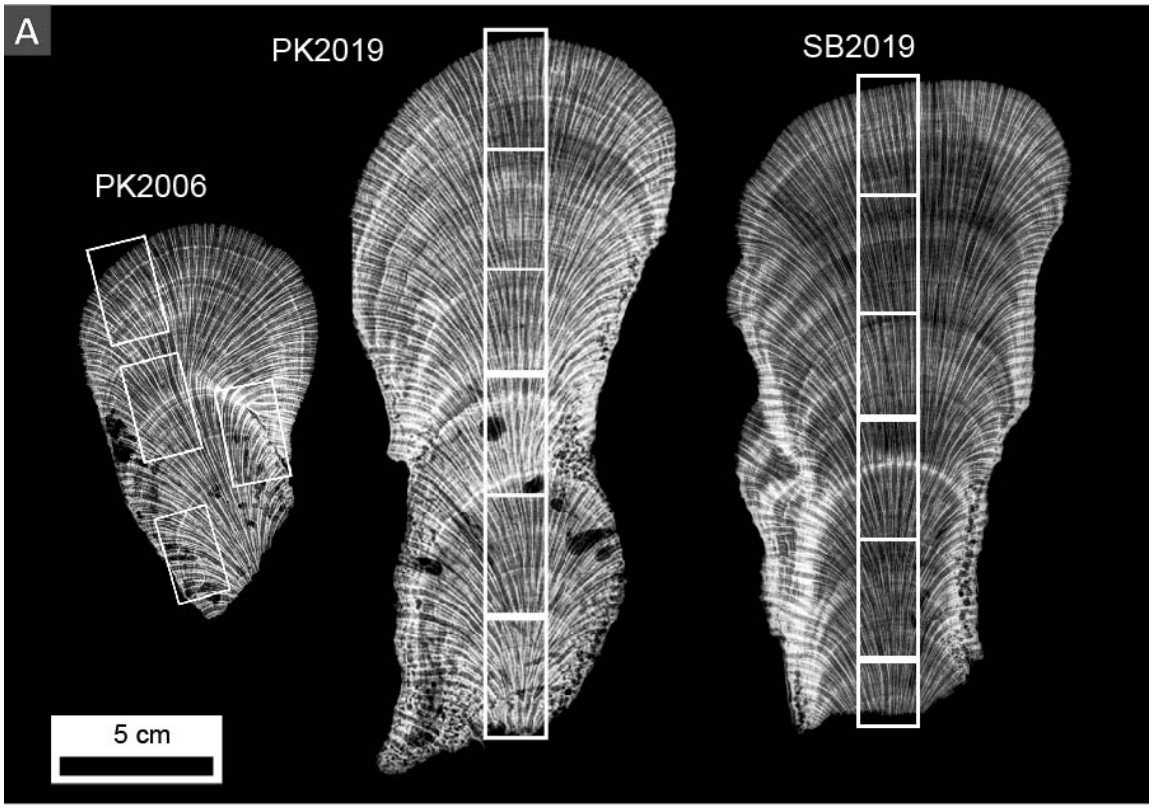
A
PK2019
SB2019
PK2006
5 cm

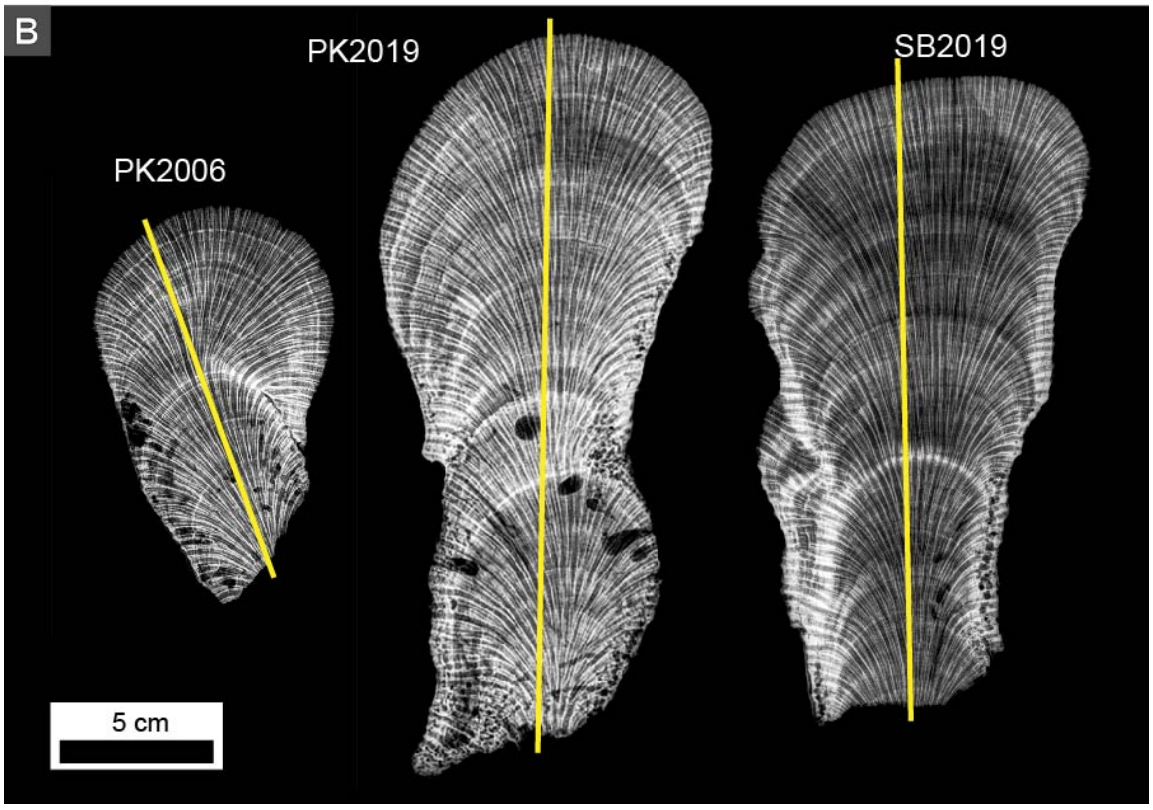
B
PK2019
SB2019
PK2006
5 cm

Figure 3. X-radiographs of 5 mm-thick vertical slices of *O. annularis* heads. Coral skeletal density banding (CSDB) is shown as alternating high-density bands (HDBs, light gray to white layers) and low-density bands (LDBs, dark gray to black layers). (**A**) White boxes indicate locations at which billets were cut to prepare standard-sized petrographic thin sections. (**B**) Yellow lines indicate location and orientation of line profile analyses presented in Figures 4 and 5.

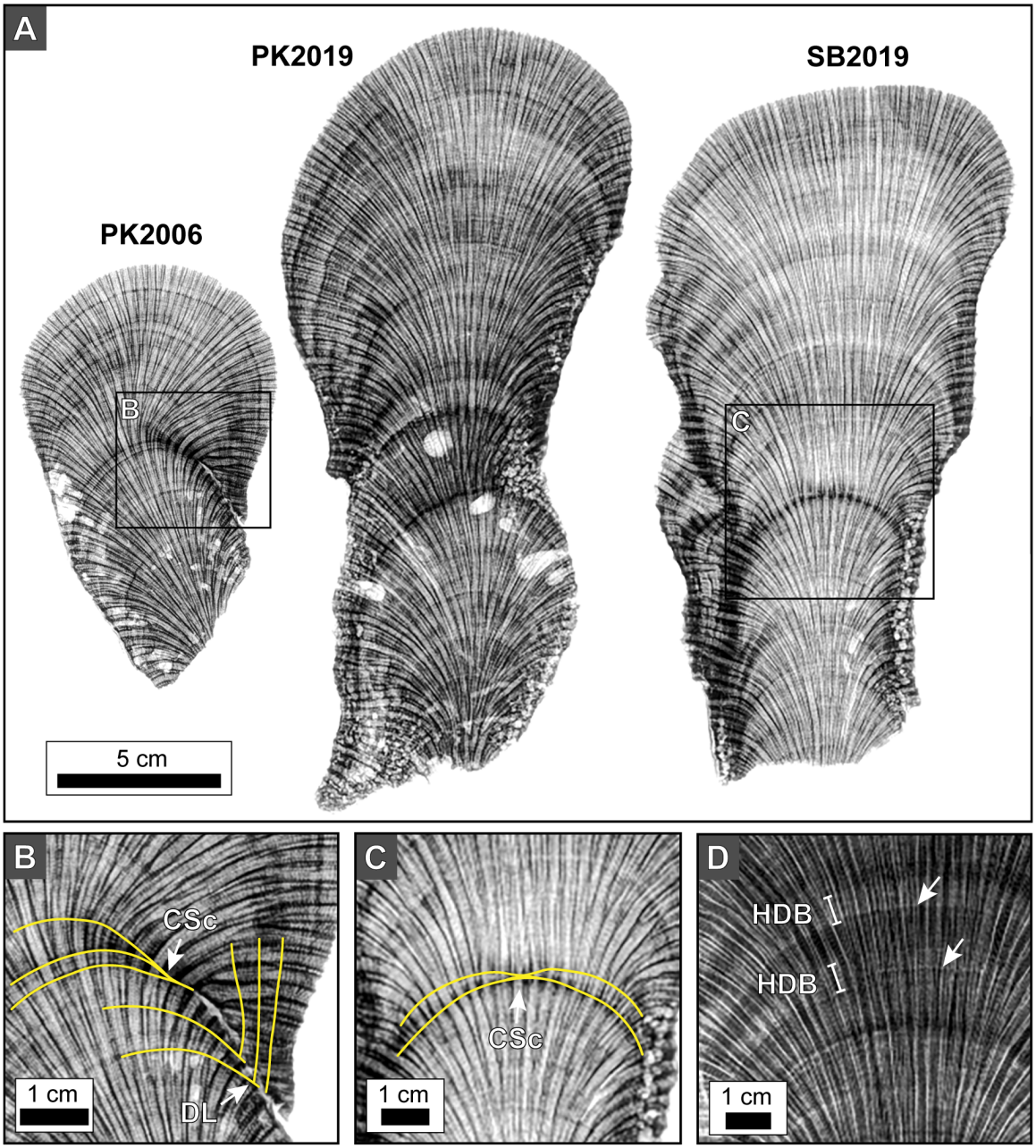

Figure 4. Inverted X-radiographs of 5 mm-thick slices of *O. annularis* heads. (**A**) PK2006, PK2019, and SB2019 coral skeleton slices. Coral skeletal density banding (CSDB) is shown as alternating high-density bands (HDBs, dark gray to black layers) and low-density bands (LDBs, light gray to white layers). Large white irregular to circular shapes in the skeletons are borings. The gap on the right side of the PK2006 skeleton represents the

hiatus surface shown in detail in Figure 5. (**B**) Enlargement of PK2006 in **A** with yellow lines tracing CSDB stratigraphy. Layers become thinner, condensed, and pinch out laterally (condensed section labeled CSc) and layers terminate against previously deposited layers (downlap labeled DL). (**C**) Enlargement of SB2019 in **A** with yellow lines tracing CSDB stratigraphy. Note the condensed HDB section in the middle of the head where no LDB formed. (**D**) Enlargement of a normal x-radiograph images of SB2019 CSDB stratigraphy. Note relatively thick HDBs and LDBs, each of which are in turn composed of finer HDBs and LDBs (white arrows).

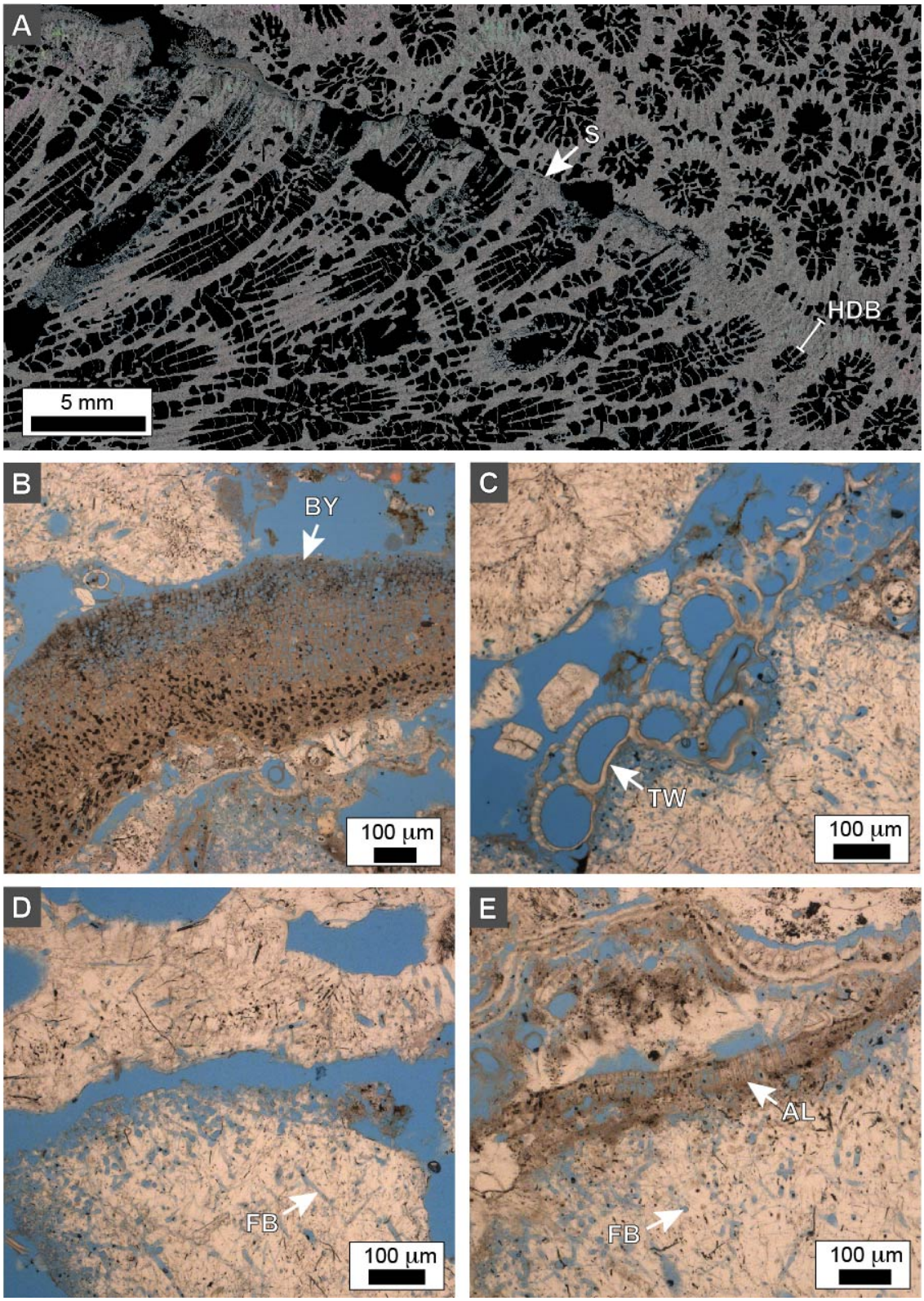
A
S
HDB
5 mm
B
BY
100 µm
C
TW
100 µm
D
FB
100 µm
E
AL
FB
100 µm

Figure 5. Photomicrographs of the *O. annularis* PK2006 hiatus surface**.** (**A**) Polarization (POL) photomicrograph of the lateral transition from the hiatus surface (S) into a pronounced age-equivalent HDB layer. Note that corallites directly below the hiatus surface are truncated and corallite growth orientation above the hiatus surface is completely different. Conversely, corallite growth is continuous across the HDB that is laterally equivalent to the hiatus surface. However, the corallite growth trajectories are significantly different above the HDB. (**B**-**E**) Brightfield (BF) photomicrographs of encrusting organisms on the hiatus surface including bryozoans (BY), serpulid tube worms (TW), fungal borings (FB), and coralline algae (AL).

CSDB layering has a tighter curvature within narrower lowermost regions of each head relative to the broader curvature within the wider regions (Figs. 2, 3, 4). In all three coral heads, HDBs and LDBs are slightly thicker in the center and become slightly thinner toward the margins (Figs. 2, 3, 4). Thick HDBs and LDBs are composed of microlayers that follow the orientation of primary CSDB stratigraphy (Fig. 4D). This is the result of condensed section in HDBs and LDBs stratigraphy (Figs. 2, 3, 4). At their margins, the skeletons exhibit several ≤1 mm-diameter bore holes that cross-cut the original CSDB stratigraphic sequences (Figs. 2, 3, 4). Larger bore holes also occur deeper in the interior of each head (lower half of PK2019 in Fig. 4). Prominent vertically radiating patterns are primarily skeletal walls (*thecal walls*) at the margin of the skeletal cups (*corallites*) that house the living coral polyps (Fig. 4). The CSDB stratigraphy is oriented perpendicular to the skeletal walls (Fig. 4).

Comparison of HDB Layers Between Coral Heads

Line profiles of the microCT and x-radiograph images exhibit a large number of peaks and troughs with variable intensities and thicknesses (Figs. 6, 7). CLAHE line profiles exhibit higher amplitude peaks and troughs (red lines on Figs. 6, 7) compared to the average line profiles (blue lines on Figs. 6, 7). This is because the CLAHE software accentuates the contrast between black and white image pixels. All line profile peaks represent HDBs (white bands) and troughs are LDBs (dark gray to black bands) (Fig. 6, 7). By combining visual observations (Fig. 4), with consistency between the average and CLAHE line profiles (Figs. 6, 7), a few HDB layers appear more prominent than others.

Prominent HDB layers were distinguished solely by the identification of bright white bands in the coral skeleton (Figs. 2, 3, 6, 7) as previous studies have done (e.g. Knuston et al. 1972; Barnes and Lough 1989; Carricart-Ganivet 2007). The precise boundaries of HDBs are hard to identify as there are cm-scale layering patterns composed with mm-scale layering (Fig. 4D). In this study, both cm-scale and mm-scale HDBs are analyzed.

In general, the x-radiograph line profiles are more accurate with identifying prominent HDBs than the microCT line profiles (Figs. 6, 7). The high-resolution spatial resolution microCT analysis prevented the microCT line profile from detecting much of the high-frequency CSDB layering except for bright prominent HDB peaks (black arrows in Figs. 6). A contributing factor to this is the fact that there was not enough time for the 2% sodium hypochlorite solution to fully remove the organic matrix within PK2019 and SB2019 (Fig. 6). Despite this, two prominent HDB peaks in PK2019 and one prominent HDB peak in SB2019 were detected (black arrows in Fig. 6). In addition, major HDB peaks are located within 3 cm of the bottom of each 2019 head (Fig. 6). The lowermost major peaks at the bottom of PK2019 and SB2019 CLAHE are false peaks due to the contrast between the skeleton and background (Fig. 6). On the other hand, X-radiograph line profiles more accurately identify the HDB peaks (Fig. 7) seen in the inverted x-radiographs (Fig. 4). There is more consistent spacing of HDB peaks and LDB troughs in x-radiographs that reflect the overall CSDB stratigraphic sequence (Fig. 7). Overall, prominent HDB layers may possibly correlate between the three coral heads (black arrows in Fig. 7). However, evaluation of potential correlation awaits quantitative statistical analysis and additional absolute dating that is not presently available for these modern corals.

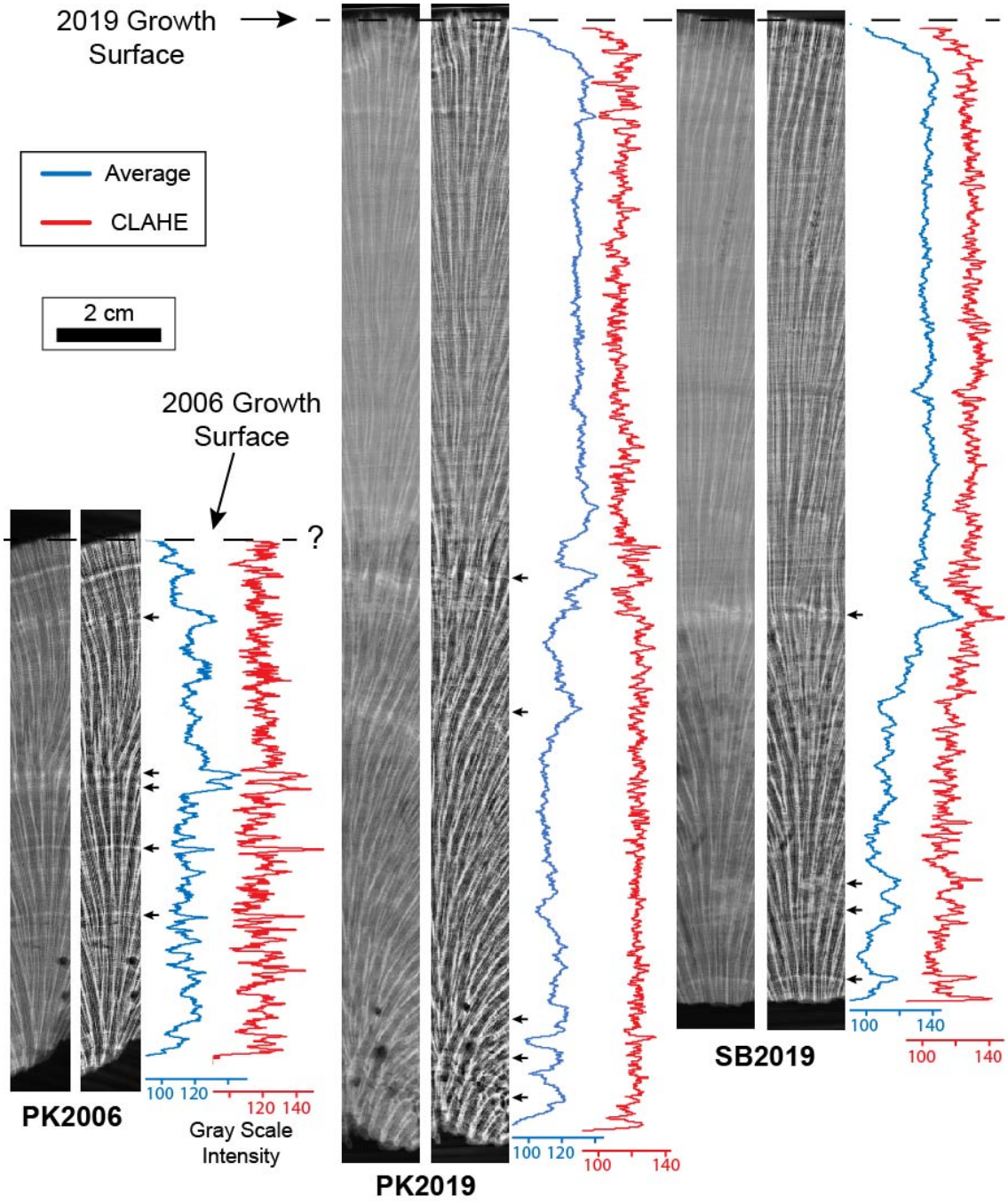

Figure 6. MicroCT image strips and line profiles of *O. annularis*. Line profile analyses were collected from vertical transects in the center of each cropped microCT image. Refer to Figure 2B for precise location of each vertical transect within each coral head. Blue line

profiles are average intensity volume projections and red line profiles are Enhanced Local Contrast (CLAHE) intensity volume projections. Small black arrows represent prominent HDB peaks distinguished by the bright white HDB layers in the adjacent image. Known outermost growth surfaces at the time of sampling in 2006 and 2019 are shown with black dashed lines. Major peaks at the base of PK2019 and SB2019 CLAHE plots (<0.5 cm from the base) are interpreted as false peaks due to the contrast between the skeleton and background.

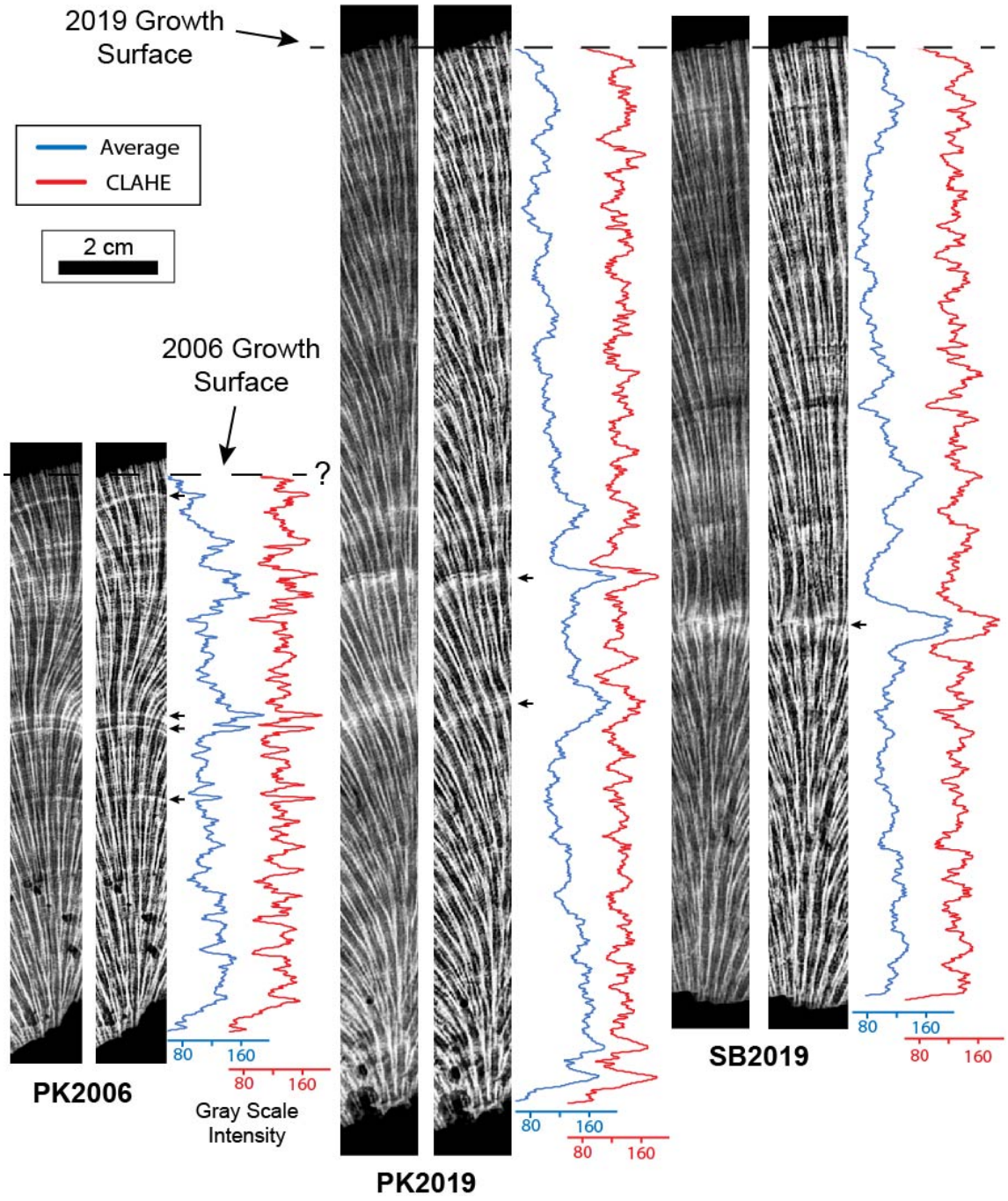

Figure 7. X-radiograph image strips and line profiles of *O. annularis*. Line profile analyses were collected from vertical transects in the center of each cropped x-radiograph image. Precise location of each vertical transect within each coral head is shown in Figure 3B.

Blue line profiles are average intensity volume projections and red line profiles are Enhanced Local Contrast (CLAHE) intensity volume projections. Small black arrows represent prominent HDB peaks distinguished by the bright white HDB layers in the adjacent image. Known outermost growth surfaces at the time of sampling in 2006 and 2019 are shown with black dashed lines.

Original Skeletal Structure and Nomenclature of *O. annularis*

Detailed micro- and nanoscale skeletal structural analyses of *O. annularis* coral skeletons have been used to determine the numerical taxonomy and the evolutionary relationship of *O. annularis* with other coral species (e.g. Stolarski and Roniewicz 2001; Budd et a. 2012; Kitano et al. 2014). Skeleton nomenclature and architecture are discussed in the following section in order to accurately analyze coral skeleton architecture in the context of CSDB stratigraphy. The individual skeletal cups (corallite or calyx) in which the *O. annularis* polyp sits, is on average 2.3 mm in diameter and contains 24 radially-distributed vertical skeletal walls (*septa*) within each corallite that support and anchor the living polyp based on previous research (Fig. 8; Weil and Knowlton 1994; Budd et al. 2012). Spacing between corallites in *O. annularis* is approximately 2 mm in *O. annularis* (Weil and Knowlton, 1994). The *Orbicella annularis* skeleton in thin section exhibits the original coral skeletal architecture secreted by multiple individual polyps within the coral animal. The complex crystalline microstructure of *O. annularis* skeletons has been studied in detail and combined with molecular analyses to determine the phylogenetic history of the Family Merulinidae (Budd et al. 2012). In the present study, the names of individual skeletal elements will follow the nomenclature presented in Budd et al. (2012).

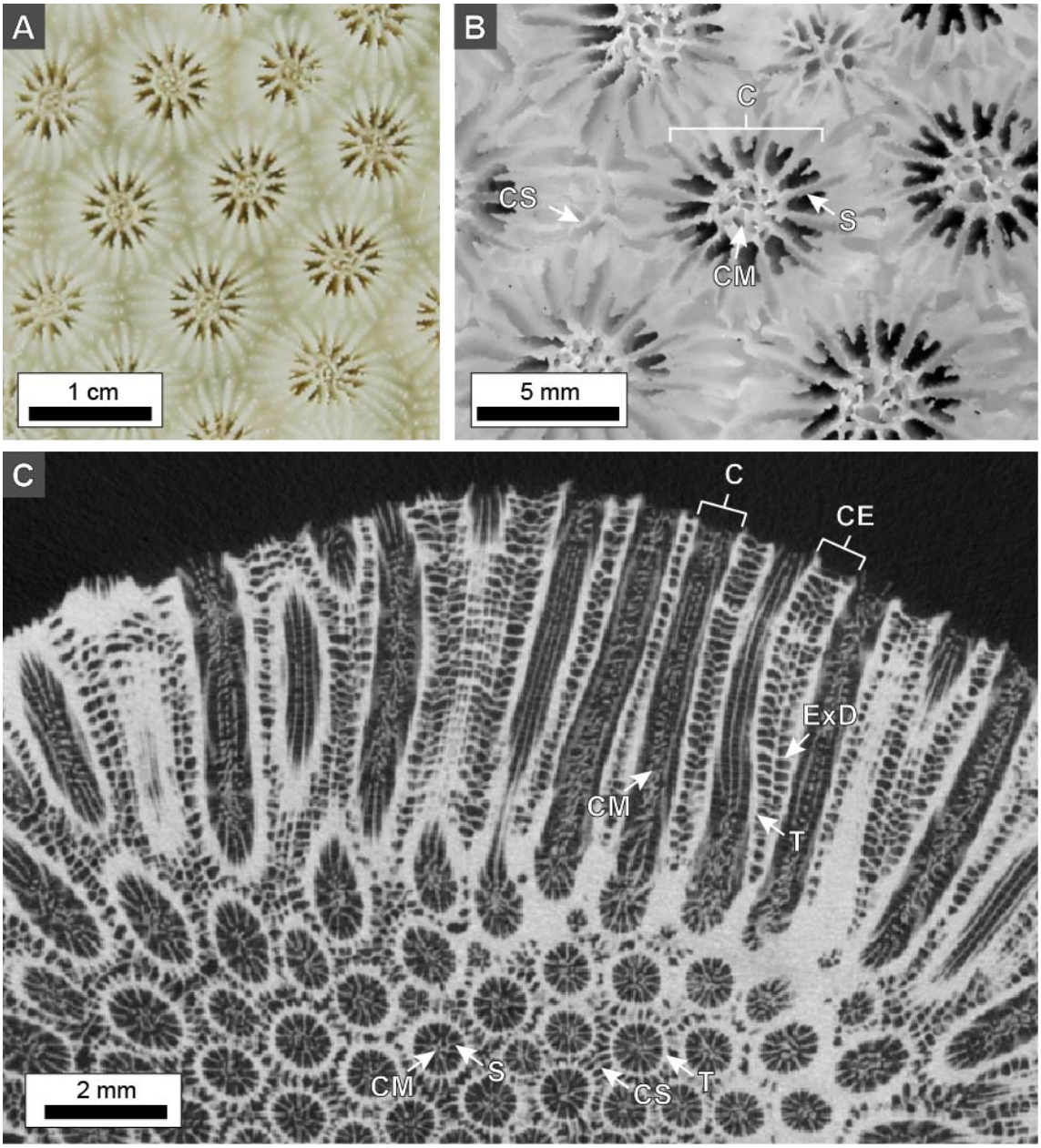

Figure 8. Terminology for skeletal components in *O. annularis*. (**A**-**B**) Photographs of the PK2006 coral skeleton surface showing the corallite (C), septa (S), columnella (CM) and costae (CS) skeletal components. (**C**) Horizontal virtual microCT cross section from PK2006 showing the corallite (C), theca (T), septa (S), columnella (CM), coenosteum (CE), costae (CS), and exothecal dissepiment (ExD) skeletal components. Note the distinct shift in growth trajectory within just a few millimeters.

The coral skeleton thin sections are dominated by individual skeletal cups (*corallites*) composed of various complex elements (Fig. 8). Individual coral polyps form corallites through secretion of an aragonite ($CaCO_3$) skeleton for structural support. A single coral animal can include hundreds to thousands of coral polyps and corallites that form a rigid skeleton. Approximately 50 μm-thick circular walls (*theca*) define the edge of a single corallite in thin section (labelled T in Fig. 8C). Theca are often jagged and thicker than the surrounding skeletal elements in order to provide adequate support for the coral polyp (Fig. 8). Corallites are composed of smaller skeletal features that lie within the theca (*endothecal*) and outside the theca (*exothecal*). Major skeletal endothecal components include 5 μm-thick vertical walls (*septa*) that radially grow from the theca, irregular and globular structures (*columnella*) in the center of the corallite, and thin ~0.5 μm-thick horizontal skeletal elements (*endothecal dissepiments*). The exothecal skeletal elements form in the space between different corallites (*coenosteum*). On the surface of the skeleton, small ridges (*costae*) run between corallites and connect to the theca and septa within a corallite (Budd et al. 2012; Fig. 8B). As the coral grows, costae walls form as the coral skeleton grows vertically upwards that provide structural support for the overall skeleton and to maintain the shape of the skeleton (labelled CS in Fig. 8 B, C). 1-2 μm-thick horizontal skeletal elements (*exothecal* dissepiments) form between the costae walls (Fig. 8).

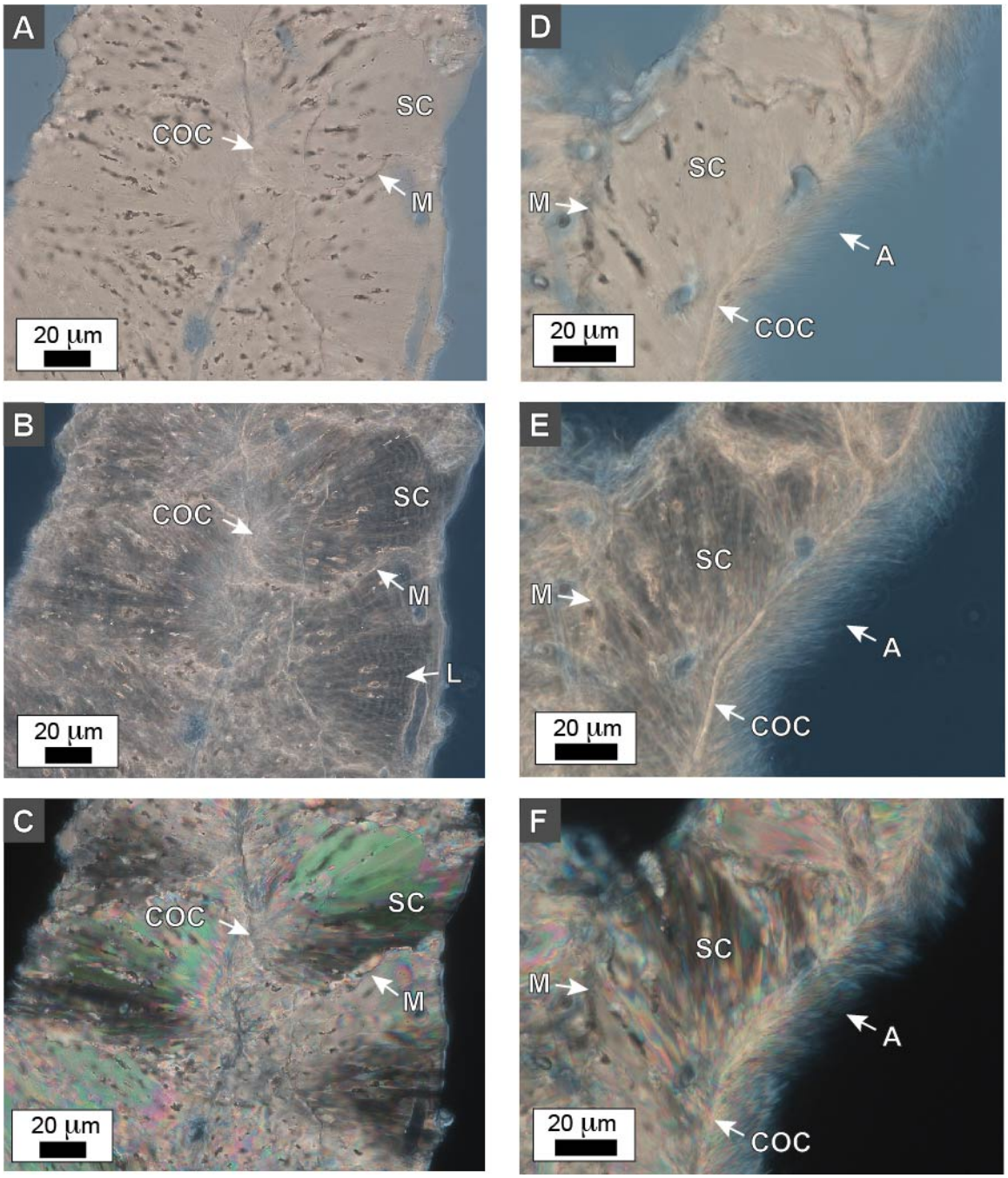

Figure 9. Photomicrographs of costae and exothecal dissepiments in *O. annularis*. (**A-C**) A representative costae cross-section photomicrograph in (**A**) brightfield (BF), (**B**) phase contrast (PC), and (**C**) polarization (POL). Multiple centers of calcification (COC) occur along the center of the costae. Sclerodermite (SC) aragonite needle bundles radiate from each COC and combine to form the costae. Fine concentric layering (L) occurs within the

sclerodermites. Individual sclerodermites abut and terminate against each other along their margins (M). (**D**-**F**) A representative cross-section of the attachment of an exothecal dissepiment to a costae in (**D**) BF, (**E**) PC, and (**F**) POL. Each dissepiment is composed of small COCs that form several sclerodermites (SC) which connect to the costae at a defined margin (M). The bottom side of the dissepiment is lined with fine 2-3 μm-thick acicular aragonite needles (A).

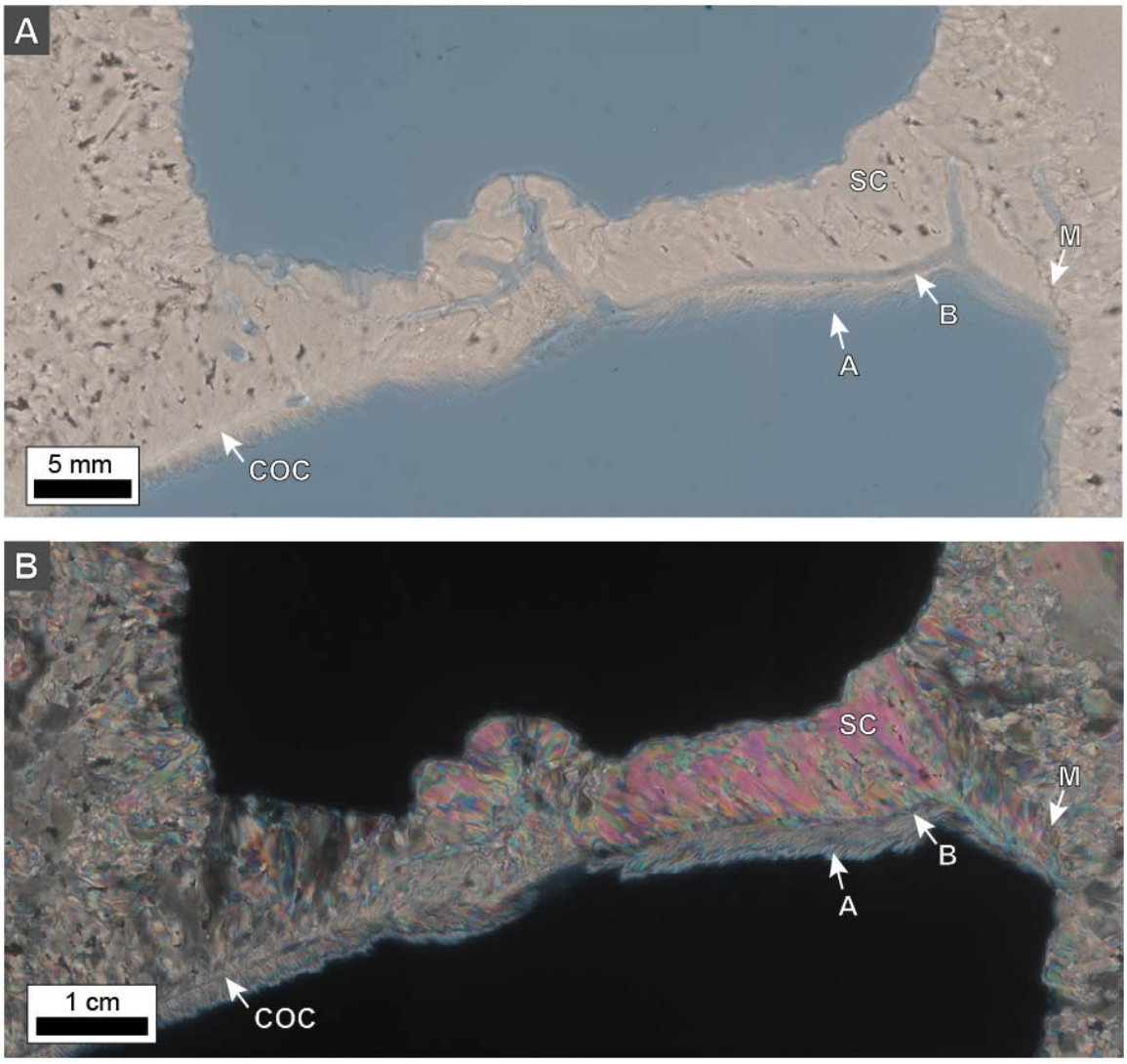

Figure 10. Photomicrographs of an exothecal dissepiment in *O. annularis*. (**A**) Brightfield (BF) and (**B**) polarization (POL). The dissepiment exhibits a sharp contact (M) with the costae on either side. Centers of calcification (COC) and sclerodermites (SC) grow horizontally away from the costae and eventually abut in the center to form an exothecal dissepiment. Directionality of growth is indicated by the orientation of aragonite needles in the sclerodermites in the dissepiment pointing away from the costae. Fine aragonite needles (A) line the bottom side of the dissepiment. Borings (B) occur along the entire dissepiment and the costae walls. The borings appear to track the distribution of COCs in the dissepiment.

Due to the multiple directions coral polyps grow on the seafloor, the corallite and coenosteum are cut at various different angles from oblique to nearly vertical cross sections of the skeletal structures. In an oblique cut, the circular corallite structure is distorted to an oblong shape with thin septal walls pointing towards the center of the corallite (Fig. 8). In a subvertical cross section view, the long subvertical to vertical columns of theca and columnella are shown (Fig. 8C). The columella is located in the center of the corallite and can be tracked down through the corallite (Fig. 8C). Horizontal endothecal dissepiments are fragile and connect to the septa, theca, and columnella within each corallite. Septa are not present in the subvertical cross section view. The coenosteum structure is not highly distorted due to the various orientation of skeleton cuts. Exothecal dissepiments and costae walls form multiple, adjacent ladder-like structures that are 0.5 mm in width (Fig. 8C).

The corallite and coenosteum structures consist of multiple 5-20 μm-diameter bundles of needle-like (*acicular*) aragonite crystals that grow from regions of granular (*microcrystalline*) aragonite crystals (Figs. 9A-C). The microcrystalline aragonite region was termed by Ogilvie 1896 as a *center of calcification (COC)* which is the terminology that will applied in this study. COCs create a pathway through the theca and costae walls as the coral polyps secrete new skeleton and grow upwards from the seafloor (Figs. 9A-C). An individual COC region produces a fan-shape cluster of acicular aragonite crystals (*sclerodermite*) that grows horizontally away from the COC in all directions (labelled SC in Figs. 9A-C). 0.1 μm-thick high frequency layering is produced in the sclerodermites as they grow towards the outside of the skeleton walls (Fig. 9B). As the walls in the skeleton grow upward through time, multiple sclerodemites grow and collide with one another to

produce a distinctive margin defined by microcrystalline aragonite cement (labelled M in Fig. 9). These sclerodermites meld together to create the robust, structurally-supported theca and costae walls that define the corallite and coensteum regions of the coral skeleton.

The endothecal and exothecal dissepiments in the coral skeleton utilize the same building block elements of COC and sclerodermites as the skeletal wall structures (Figs. 9D-F, 10). The dissepiments consist of two pathways of COCs that connect to two adjacent theca and/or costae walls (Fig. 10). At the edges of the dissepiment, a COC grows upward at an oblique angle into the pore space of the skeleton. As the COC pathway is tracked across the dissepiment, the COC orientation becomes horizontal (Figs. 9D-F, 10). The orientation of the aragonite crystals within sclerodermites follow the same pattern as the COCs in the dissepiment (Figs. 9D-F, 10). The sclerodermites abut against the theca and/or costae walls and form a margin between the dissepiment and the skeletal wall (labelled M in Figs. 9D-F, 10). In the center of the dissepiment, the orientation of the aragonite needles in the sclerodermites become pointed upward (Fig. 10). The underside of the dissepiment is nearly completely covered by ~500 nm-thick acicular aragonite crystals (labelled A in Figs. 9D-F, 10). These thin aragonite crystals grow on top of COCs (Figs. 9D-F, 10).

Thickened Skeletal Walls and Dissepiments within HDBs

Under high resolution thin section microscopy, density bands within the CSDB stratigraphy are original skeleton bands. Original skeleton density bands are composed of differences in the thickness of exothecal dissepiments and costae walls moving vertically through the skeleton. The skeletal elements in the exothecal areas are consistently thicker

in HDBs than LDBs (Fig. 11). The slight variations of thickness are further expressed and more readily shown in a 5 mm slice of coral skeletons to create different density layers observed in CSDB stratigraphy. Three prominent HDBs in the PK2019 and SB2019 coral skeletons show abnormally thickened costae walls that form denser HDBs (Fig. 12). No exothecal dissepiments are developed in these bands as the costae walls are overthickened and adjacent walls abut against one another (Fig. 12C-F). The aragonite crystals in sclerodermites point toward each other and abut against one another to form an irregular margin between adjacent costae walls (Fig. 12E, F). As a result, pore space between the costae walls are not formed to produce a bright, white HDB in standard XRD (Fig. 12A, B). The thickened skeletal walls are not horizontally continuous across the prominent band as the endothecal dissepiments and columnella elements maintain their shape and regular thickness (Fig. 12D, F). The pore space within the endothecal area is maintained as well. Another type of band, diagenetic bands, has been observed within *Porites* coral species on the Great Barrier Reef in Australia (Sivaguru et al. 2019). During the present study these digenetic bands were not observed within the three *O. annularis* coral skeletons.

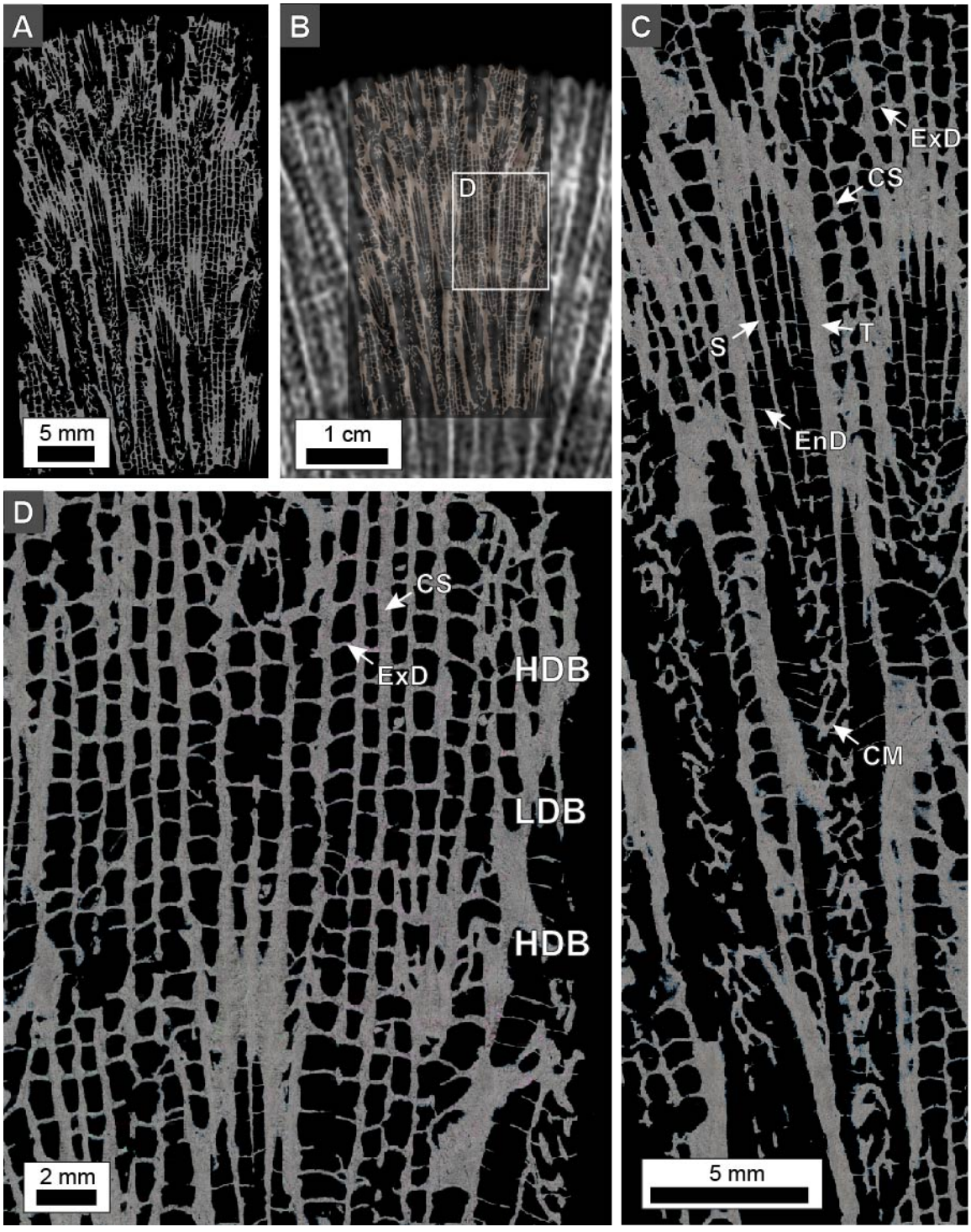
A
5 mm
B
D
1 cm
C
ExD
CS
S
T
EnD
CM
5 mm
D
CS
ExD
HDB
LDB
HDB
2 mm

Figure 11. Polarization (POL) photomicrographs of *O. annularis* cross-sections. Sample collected from the uppermost 2 cm of the PK2019 head (location shown in Fig. 3A). (**A**) Image of the entire thin section. (**B**) Thin section overlain on the x-radiograph image from the same location. This technique permits precise spatial orientation of the position of HDBs and LDBs on the thin section, which can only be identified with x-radiographs. White box denotes enlarged area shown in **D**. (**C**) Enlargement of a corallite cross-section. Skeletal structures shown include theca (T), septa (S), columnella (CM), endothecal dissepiment (EnD), costae (CS), and exothecal dissepiment (ExD). (**D**) Cropped enlargement of the coenosteum skeletal structures that include exothecal dissepiments (ExD) and costae (CS). Note that exothecal dissepiments and costae are substantially thicker in HDBs and thinner in LDBs.

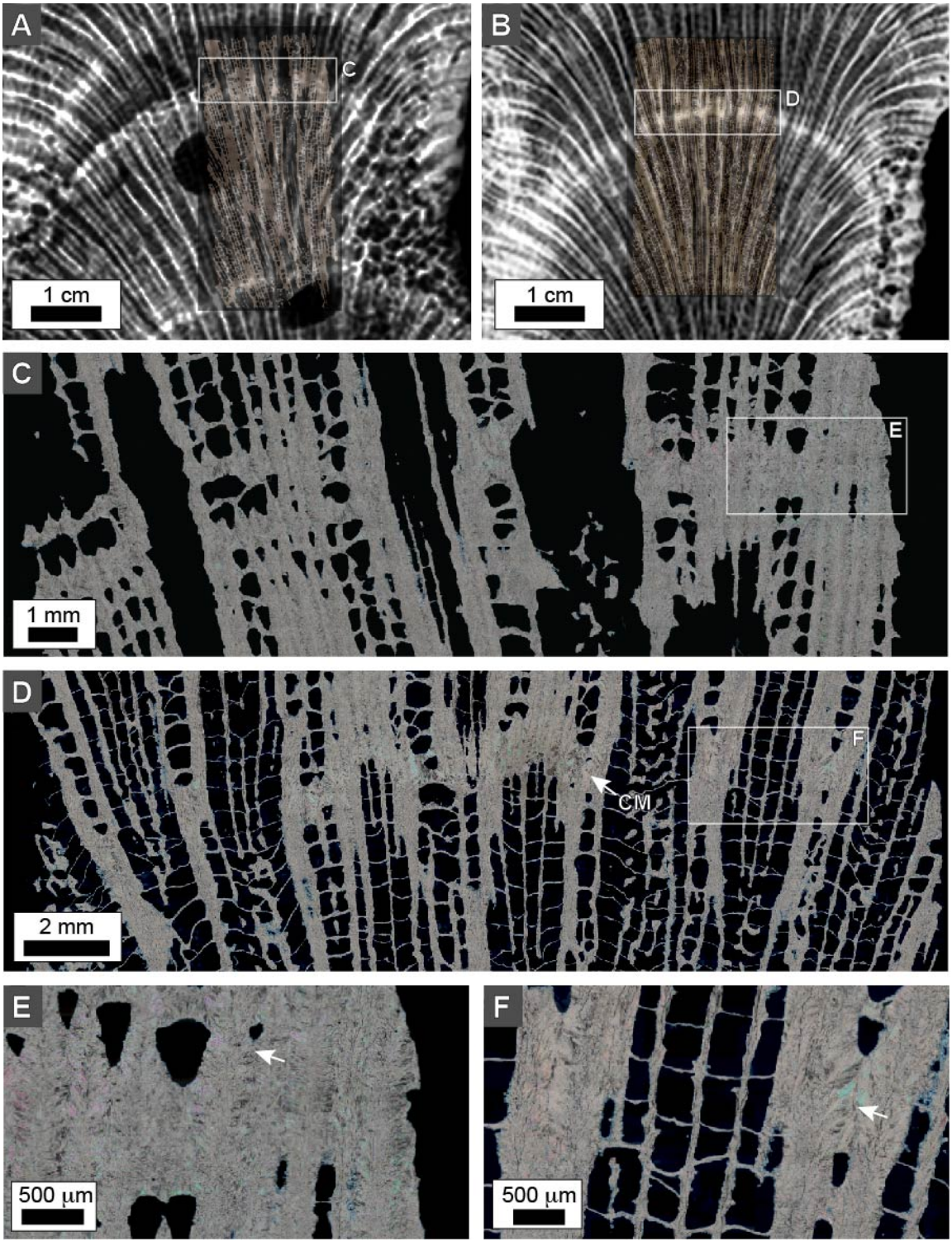
A
C
1 cm
B
D
1 cm
C
E
1 mm
D
F
CM
2 mm
E
500 μm
F
500 μm

Figure 12. Polarization (POL) photomicrographs of *O. annularis* cross-sections. From 10 cm below the growth surface of the PK2019 and SB2019 *O. annularis* heads (location shown in Fig. 3A). (**A**) Thin section overlain on the PK2019 x-radiograph image from the same location. This technique permits precise spatial orientation of the position of HDBs and LDBs on the thin section. White box denotes enlarged area shown in **C**. (**B**) Thin section overlain on the SB2019 x-radiograph image from the same location. This technique permits precise spatial orientation of the position of HDBs and LDBs on the thin section. White box denotes enlarged area shown in **D**. (**C-D**) Cropped images showing overthickened skeleton in HDB layers in the (**C**) PK2019 and (**D**) SB2019 skeletons. Pore space within the coenosteum (CM) HDB is absent, while HDBs within the corallite have pore space. White boxes indicate areas of enlargement shown in **E** and **F**. (**E-F**) Enlargements showing lack of porosity between costae in (**E**) PK2019 and (**F**) SB2019. White arrows show overthickened costae that abut against each other.

DISCUSSION

Skeletal Thickening Forms HDBs

While a detailed understanding of the combined biotic and abiotic mechanisms that control HDB formation is not yet completely understood, several hypotheses have been proposed. In general, it has been shown that HDBs form during high SST and LDBs form during low SST (Knuston et al. 1972; Barnes and Lough 1989; Sayani et al. 2011). It is generally thought that zooxanthellae photosynthetic activity is increased during high SST and therefore CO_2 drawn down is increased (Berkelmans and van Oppen 2006). This causes an increase in saturation state of fluids within the calicoblastic epithelium where the aragonite skeleton is precipitated (Allemand et al. 2011). This results in more precipitation of aragonite skeletal material. Conversely, LDB layers form when zooxanthellae photosynthetic activity is decreased during lower SST, decreasing CO_2 drawn down (Berkelmans and van Oppen 2006), and lowering the aragonite saturation in the calicoblastic epithelium (Allemand et al. 2011). This hypothesis does not take into account extremely high SST that would lead to a decrease in photosynthetic activity and lead to coral bleaching.

High-resolution thin section petrography in the present study reveals for the first time that HDBs are formed by the thickening of skeletal elements in the coenosteum outside of the corallites. These coenosteum skeletal elements include theca, costae, and exothecal dissepiments. Conversely, the endothecal dissepiments and septa structures within individual corallites do not thicken. This evidence requires that HDBs are formed in times of increased aragonite saturation. This is consistent with previous experiments

showing that zooxanthellae photosynthetic activity is enhanced as SST is increasing, prior to reaching a maximum after which photosynthetic activity decreases (Fitt et al. 2001; Rowan 2004; Berkelmans and van Oppen 2006). The variability and rate of SST increase would in turn explain the wide variation observed in the thickness, intensity, and frequency of HDBs within overall CSDB stratigraphic patterns (Figs. 4, 11, 12).

CSDB Stratigraphy Reflects Coral Ecology

Previous studies using CSDB to reconstruct paleoclimatic estimates of SST have made several untested assumptions (e.g., Lough and Barnes 1989; De'ath et al. 2009; Alpert et al. 2016). For instance, CSDB sequences of HDBs and LDBs have been assumed to represent continuous, undisrupted growth of the coral skeleton (e.g. Knuston et al. 1972; Lough and Barnes 1989; Cruz-Piñón et al. 2003). In addition, it has been assumed that the most pristine and continuous skeleton is located within the central portion of coral heads due to bioerosion observed on the margins (e.g. Hendy et al. 2007; Northdurft and Webb 2007; Alpert et al. 2016). Furthermore, each HDB-LDB couplet has been assumed to represent one-year of growth in response to a complete seasonal cycle (e.g. Knutson et al, 1972; Barnes and Lough 1989; Sayani et al. 2011). These assumptions permitted CSDB to be used as a reliable chronometer, like tree rings, and provide absolute dating for isotopic analyses. In contrast, the integration of microCT, x-radiography, and optical microscopy in the present study indicates that CSDB reflects an extremely complicated growth history. As documented in the following discussion, HDB-LDB couplets do not represent simple

annual variations in SST and significant hiatuses occur within CSDB stratigraphic sequences.

This is the first study to apply well-established geologic stratigraphic concepts from strategically sampled coral heads to interpret the relative timing of *O. annularis* CSDB sequences. Results indicate that each head represents a complex history of changing coral growth and ecological conditions (Fig. 13). A striking example of a CSDB layer that represents a loss of time (*hiatus surface*) is observed in PK2006 (Figs. 4, 5, 13). In the middle of the CSDB sequence, the coral experienced a significant lateral shift in the location of skeletal growth (Fig. 13). Coral tissue was removed from a third of the coral surface, then encrusted, bored, and bioeroded by multiple benthic organisms including bryozoa, coralline algae, serpulid tube worms, and fungi (Fig. 5). Corallites directly below the hiatus surface are truncated and corallite growth orientation above the hiatus surface is in a different direction (Figs. 5, 13). At the same time, healthy coral growth continued on lateral, age equivalent stratigraphic surfaces (Figs. 4, 5, 13). This lateral shift in coral growth is further indicated by the down lap and condensed CSDB sections at the margins of the coral head (Figs. 4B, 4C, 13). These types of stratigraphic relationships are also exhibited in PK2019 and SB2019 (Fig. 4). Growth continued laterally to the hiatus surface and eventually deposited skeleton on top of the encrusted and bioeroded unconformity. This is shown by the lateral continuity of CSDB layers across the entirety of the head, which are also deposited on top of the hiatus surface. This explains the observed CSDB stratigraphy in which a prominent HDB layer is laterally equivalent to the encrusted and bored hiatus surface (Figs. 4, 5, 13).

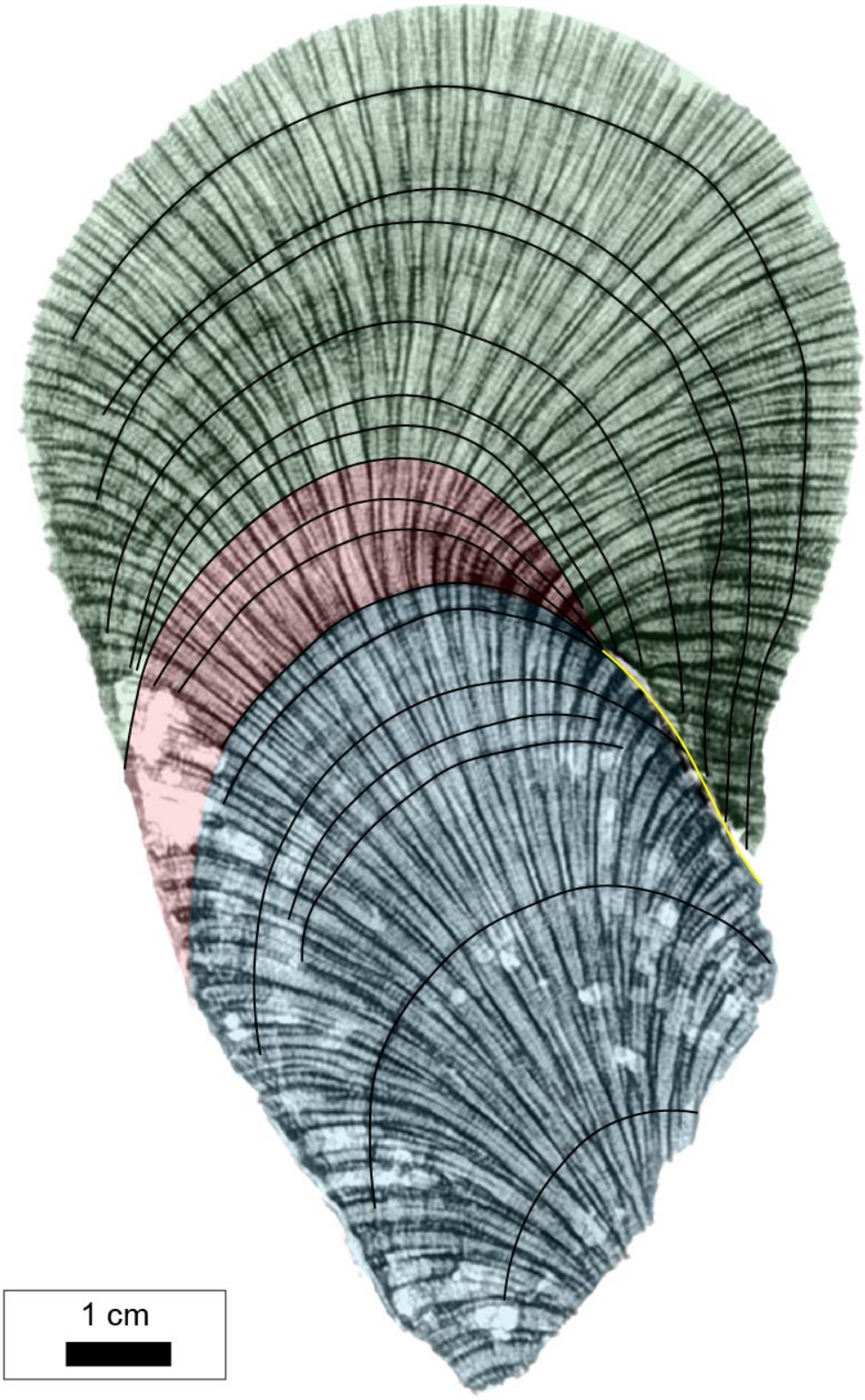
1 cm

Figure 13. Coral Skeletal Density Banding (CSDB) Growth History of PK2006. Inverted x-radiograph of the PK2006 5 mm thick skeleton slice. The skeleton is divided into three sections: skeletal growth before the hiatus event (blue), skeletal growth during the hiatus event (red), and skeletal growth after the hiatus event (green). The thin yellow line between the blue and green regions denotes the hiatus surface. Note condensed section of CSDB layers in the red region that represent the continued growth of skeleton laterally adjacent to the hiatus surface. Thin black lines represent prominent HDB layers that are easily identified on the inverted x-radiograph. to display the CSDB stratigraphy in the three separate growth regions.

Although uncertain because absolute age dating is not available, it is likely the lateral shift in coral growth and the duration of the hiatus may represent approximately one- to two-year time span. This is based on the ~1 cm thick coral skeleton that grew after it shifted to the left in the image but before it shifted back to cover the hiatus surface (Fig. 13). Given that the average skeletal growth rate for *O. annularis* is 0.5-2.6 cm/yr based on direct measurements of growth rates (Madin et al. 2016), the hiatus formed over an approximately 1 to 2 year period of time.

Another striking example of a hiatus is shown in the center of the SB2019 skeleton where LDB layers onlap and form a condensed section on the underlying HDB layer (Fig. 4C). Directly above the prominent HDB layer in the middle of SB2019, the LDB layer is pinched out in the middle of the head (Fig. 4C). In all three heads, small-scale (< 3 mm) lateral variations in HDB-LDB couplet thickness within age equivalent layers indicates that variable growth rates occurred across the same growing surface of the coral head at any one time (Figs. 4, 13). Thus, the layering sequences and patterns need to be fully addressed to determine the relative timing of HDB-LDB couplets before taking precise isotope measurements for paleoclimatic reconstructions.

Throughout the three coral heads, distinct HDB-LDB couplets in the CSDB sequences may not represent one year of coral growth. The average skeletal growth rate for *O. annularis* is 0.5-2.6 cm/yr (Madin et al. 2016). The growth rates used from Madin et al. (2016) were taken from studies that recorded direct, in situ measurements of coral skeleton through time. For example, Cruz-Piñón et al. (2003) inserted a stainless steel surgical needle in multiple *O. annularis* coral heads to track skeletal growth over one year.

Therefore, it is directly known that the minimum average skeletal growth rate is 0.5 cm/yr. In the present study, HDB-LDB couplet thickness varies across CSDB stratigraphic sequences. However, all three coral heads exhibit distinct HDB-LDB couplets that are less than 0.5 cm thick (Figs. 4, 13). Assuming the previously reported minimum growth rates are accurate, this observation indicates that certain HDB-LDB couplets may form in less than one year and do not represent one year of coral growth. This result is significant as previous studies assume HDB-LDB couplets represent one year of coral growth when reconstructing decades-long SST from vertical transects of skeletal chemistry preserved within CSDB layering. If certain HDB-LDB couplets form in less than a year, it can be a source of error as there would inaccurate dating of CSDB-derived SST models. Thus, it is paramount to compare HDB-LDB couplet thicknesses in CSDB stratigraphic sequences with known coral skeletal growth rates to determine whether CSDB accurately dates coral skeletons and isotopic measurements.

Dynamic Coral Processes Obstruct Correlation of CSDB Sequences

Previous studies have used CSDB stratigraphy, with the collection of assumptions described above, to generally bracket and age-correlate equivalent intervals of coral skeletal growth between heads (e.g., Lough and Barnes 1989, De'ath et al. 2009, Sayani et al. 2011, Alpert et al. 2016). Within this framework, they then completed continuous transects of carbon and oxygen isotopic analyses in order to correlate paleothermometry events of SST. The present study is the first to test whether correlations can be made based solely on CSDB stratigraphic sequences. However, results from CSDB line profiles of

alternating HDBs and LDBs could not be successfully correlated between PK2006, PK2019, and SB2019 (Figs. 6, 7). The only layers for which the absolute age of formation is known are the uppermost growth surfaces of each skeleton at the time of collection. It was originally expected that, at a minimum, the PK2006 uppermost growth surface could be correlated between PK2019 and SB2019 within the context of CSDB stratigraphy. However, detailed analysis of microCT scans, inverted x-radiographs, and line profiles found no CSDB stratigraphic intervals that could be visually correlated with respect to HDB-LDB banding thickness, frequency, and peak intensities (Figs. 4, 6, 7). This further implies that CSDB stratigraphy is not solely influenced by seasonal SST variations, but instead represents highly complex interactions between the coral holobiont and changing environmental conditions. These results may help explain previous anomalies in CSDB-derived SST reconstructions (e.g. Bolton et al. 2014; Zinke et al. 2016; Krawczyk et al. 2020). The anomalies arise from the CSDB-derived SST not perfectly correlating with the recorded instrumental SST when the two data are plotted on the same graph. There is also discrepancy between different corals collected in the same region (Zinke et al. 2016).

Given these challenges in CSDB correlations between heads, hypotheses could be made in future studies by incorporating high-resolution microscopy, microCT scans, and x-radiographs with published SST data (e.g. NOAA). For instance, Curaçao experienced an Alert Level 2 30.3°C SST bleaching event in 2010, which was 1°C above the 29°C bleaching threshold SST (NOAA Coral Reef Watch 2020). This type of thermal stress event could lead to the deposition of prominent HDB layers in *O. annularis* on Curaçao. In the present study, multiple prominent HDBs were observed at a variety of stratigraphic

depths below the uppermost 2019 growth surface that could represent the 2010 bleaching event. However, the wide range in growth rates for *O. annularis* (Madin et al. 2019) precludes the correlation of any one of these HDBs with the 2010 bleaching event. Future analyses will include stratigraphically continuous transects of oxygen isotope analyses will be conducted along the line profiles for PK2006, PK2019, and SB2019 (Figs. 4, 5) in order establish paleothermometry SST reconstructions, compare the isotopic and potential CSDB correlations between the three heads, and attempt to link HDBs to prominent SST events recorded over the past 20 years.

CONCLUSION

Coral skeletal density banding (CSDB) is found in aragonitic $CaCO_3$ skeletons of tropical shallow water scleractinian "stony" corals around the world. Detected with x-ray analyses, CSDB is composed of layered couplets of high density bands (HDBs) and low density bands (LDBs). These CSDB stratigraphic sequences are commonly used as a chronostratigraphic framework within which to reconstruct sea surface temperature (SST) from coral skeleton isotopic paleothermometry. However, this approach is predicated upon several basic assumptions regarding CSDB stratigraphy that include: (1) each HDB-LDB couplet reflects one year of skeletal growth in response to seasonal changes in SST; (2) CSDB stratigraphy along the central growth trajectory of coral heads provides an undisrupted and continuous history of coral skeletal growth; and (3) the margins of coral heads yield little useful information. Correlation between heads growing in different locally, regionally and globally distributed coral reef ecosystems has relied heavily on

isotopic transects and their associated SST paleothermometry and much less on detailed CSDB stratigraphy.

The present study was undertaken to investigate these basic hypotheses regarding the formation, stratigraphic correlation, and ecological significance of CSDB crystalline architecture and stratigraphy. Three small heads of the common scleractinian coral *Orbicella annularis* growing at 8 m water depth were collected from the backreef depositional facies at Playa Kalki (2016 and 2019) and Snake Bay (2019) from the leeward reef tract of the southern Caribbean island of Curaçao. *O. annularis* was chosen for study because of it has been previously well-studied, exhibits distinct CSDB stratigraphic sequences, has been used in paleothermometry SST reconstructions, and holds ecological and geological importance to modern and ancient Caribbean reefs.

High-resolution optical petrography, overlain with CSDB x-radiographs, reveals that HDBs are created by the thickening of theca, costae, and exothecal dissepiments skeletal elements. These skeletal components form in the coenosteum, which is outside of and surrounds the corallites. Conversely, endothecal dissepiments and septa structures within corallites are not thickened. The integration of optical microscopy with microCT scans and x-radiography indicates that specific HDB-LDB couplets may not represent simple annual variations in SST. Certain HDB-LDB couplets are thinner than expected given the minimum measured skeletal gowth rate. In addition, each *O. annularis* head underwent a complicated growth history punctuated by pronounced lateral shifts in skeletal growth and hiatuses that have been encrusted and bored. These analyses indicate that CSDB stratigraphy is a sensitive crystalline record of the ecology of the host coral,

symbiotic zooxanthellae, and resident microorganisms (*coral holobiont*). Therefore, accurate CSDB-derived SST reconstructions require that these biotic processes must be factored in with annual changes in SST when calibrating predictions of future global climate change.

BIBLIOGRAPHY

Alibert, C., & McCulloch, M.T. (1997). Strontium/calcium ratios in modern Porites corals from the Great Barrier Reef as a proxy for sea surface temperature: calibration of the thermometer and monitoring of ENSO. *Paleoceanography*, v. 12, no. 3, p. 345–363. doi:10.1029/97pa00318

Allemand, D., Tambutté, É., Zoccola, D., & Tambutté, S. (2011). Coral calcification, cells to reefs. *Coral Reefs: An Ecosystem in Transition*, p. 119–150. doi:10.1007/978-94-007-0114-4_9

Alpert, A.E., Cohen, A.L., Oppo, D.W., DeCarlo, T.M., Gove, J.M., & Young, C.W. (2016). Comparison of equatorial Pacific sea surface temperature variability and trends with Sr/Ca records from multiple corals. *Paleoceanography*, v. 31, no. 2, p. 252–265. doi:10.1002/2015pa002897

Bak, R.P.M., & Luckhurst, B.E. (1980). Constancy and change in coral reef habitats along depth gradients at Curaçao. *Oecologia,* v. 47, no. 2, p.145-155.

Barkley, H.C., Cohen, A.L., Golbuu, Y., Starczak, V.R., DeCarlo, T.M., & Shamberger, K. E. F. (2015). Changes in coral reef communities across a natural gradient in seawater pH. *Science Advances*, v. 1, no. 5, e1500328. doi:10.1126/sciadv.1500328

Barnes, D.J., & Lough, J.M. (1993). On the nature and causes of density banding in massive coral skeletons. *Journal of Experimental Marine Biology and Ecology*, v. 167, no. 1, p. 91–108. doi:10.1016/0022-0981(93)90186-r

Berkelmans, R., & van Oppen, M.J. (2006). The role of zooxanthellae in the thermal tolerance of corals: a 'nugget of hope' for coral reefs in an era of climate change.

Proceedings of the Royal Society B: Biological Sciences, v. 273, no. 1599, p. 2305–2312. doi:10.1098/rspb.2006.3567

Blunden, J., & Arndt, D.S. (2017). A look at 2016: takeaway points from the state of the climate supplement. *Bulletin of the American Meteorological Society*, v. 98, no. 8, p. 1563–1572. doi:10.1175/bams-d-17-0148.1

Bolton, A., Goodkin, N.F., Hughen, K., Ostermann, D.R., Vo, S.T., & Phan, H.K. (2014). Paired Porites coral Sr/Ca and δ18O from the western South China Sea: proxy calibration of sea surface temperature and precipitation. *Palaeogeography, Palaeoclimatology, Palaeoecology*, v. 410, p. 233–243. doi:10.1016/j.palaeo.2014.05.047

Budd, A.F., Fukami, H., Smith, N.D., & Knowlton, N. (2012). Taxonomic classification of the reef coral family Mussidae (Cnidaria: Anthozoa: Scleractinia). *Zoological Journal of the Linnean Society*, v. 166, no. 3, p. 465–529. doi:10.1111/j.1096-3642.2012.00855.x

CARMABI; Caribbean Marine Biology Institute. Est. 1955. Curaçao. www.carmabi.org

Carricart-Ganivet, J.P. (2004). Sea surface temperature and the growth of the West Atlantic reef-building coral *Montastraea annularis*. *Journal of Experimental Marine Biology and Ecology*, v. 302, no. 2, p. 249–260. doi:10.1016/j.jembe.2003.10.015

Carricart-Ganivet, J.P. (2007). Annual density banding in massive coral skeletons: result of growth strategies to inhabit reefs with high microborers' activity? *Marine Biology*, v. 153, no. 1, p. 1–5. doi:10.1007/s00227-007-0780-3

Carricart-Ganivet, J.P., Cabanillas-Terán, N., Cruz-Ortega, I., & Blanchon, P. (2012). Sensitivity of calcification to thermal stress varies among genera of massive reef-building corals. *PLoS ONE*, v. 7, no. 3, e32859. doi:10.1371/journal.pone.0032859

Cohen, A.L. & McConnaughey, T.A. (2003). Geochemical perspectives on coral mineralization. *Reviews in Mineralogy and Geochemistry*, v. 54, no. 1, p. 151–187. doi:10.2113/0540151

Cruz-Piñón, G., Carricart-Ganivet, J.P. & Espinoza-Avalos, J. (2003). Monthly skeletal extension rates of the hermatypic corals *Montastraea annularis* and *Montastraea faveolata* : biological and environmental controls. *Marine Biology*, v. 143, no. 3, p. 491–500. doi:10.1007/s00227-003-1127-3

Cuif, J.P. & Dauphin, Y. (2005). The Environment recording unit in coral skeletons – a synthesis of structural and chemical evidences for a biochemically driven, stepping-growth process in fibres. *Biogeosciences, European Geosciences Union*, v. 2, no. 1, p. 61-73. ffhal-00330309

De'ath, G., Lough, J.M., & Fabricius, K.E. (2009). Declining coral calcification on the Great Barrier reef. *Science*, v. 323, no. 5910, p. 116–119. doi:10.1126/science.1165283

Debrot, A.O., & Bak, R.P.M. (2019). Brief history of CARMABI (Caribbean Research and Management of Biodiversity). In newsletter 'Historie van de oceanografie club' 16:9-18.

DeCarlo, T.M., & Cohen, A.L. (2017). Dissepiments, density bands and signatures of thermal stress in Porites skeletons. *Coral Reefs*, v. 36, no. 3, p. 749–761. doi:10.1007/s00338-017-1566-9.

Demers, C., Hamdy, C.R., Corsi, K., Chellat, F., Tabrizian, M., & Yahia, L. (2002). Natural coral exoskeleton as a bone graft substitute: a review. *Bio-Medical Materials and Engineering,* v. 12, no. 1, p. 15-35. PMID: 11847406

Desalvo, M.K., Voolstra, C.R., Sunagawa, S., Schwarz, J.A., Stillman, J.H., Coffroth, M. A. Szmanti, A., & Medina, M. (2008). Differential gene expression during thermal stress and bleaching in the Caribbean coral *Montastraea faveolata*. *Molecular Ecology*, v. 17, no. 17, p. 3952–3971. doi: 10.1111/j.1365-294x.2008.03879.x

Dornelas, M., Madin, J.S., Baird, A.H., & Connolly, S.R. (2017). Allometric growth in reef-building corals. *Proceedings of the Royal Society B: Biological Sciences*, v. 284, no. 1851, p. 20170053. doi:10.1098/rspb.2017.0053

Fessenden, M. (2014). Sea coral makes excellent human bone grafts. *Smithsonian Magazine*. Retrieved from http://www.smithsonianmag.com/smart-news/sea-coral-makes-excellent-human-bone-grafts-180953121/

Fitt, W.K., & Warner, M.E. (1995). Bleaching patterns of four species of Caribbean reef corals. The Biological Bulletin, v. 189, no. 3, p. 298–307. doi:10.2307/1542147

Flügel, E. (2004). Microfacies of Carbonate Rocks. doi:10.1007/978-3-662-08726-8

Fouke, B.W., Beets, C.J., Meyers, W.J., Hanson, G.N., & Melillo, A.J. (1996). 87Sr/86Sr Chronostratigraphy and dolomitization history of the Seroe Domi formation, Curaçao (Netherlands Antilles). *Facies*, v. 35, no. 1, p. 293–320. doi:10.1007/bf02536966

Fouke, K.W., Sivaguru, M., Todorov, L., Kingsford, M.J., Fouke, K.E., Trop, J.M., and Fouke, B.W., 2018. Crystalline structure and diagenesis of high and low density bands in Porites coral skeletons, Myrmidon Reef, Great Barrier Reef, Australia. *GSA Annual Meeting*, November, 2018.

Frias-Lopez, J., Zerkle, A.L., Bonheyo, G.T., & Fouke, B.W. (2002). Partitioning of bacterial communities between seawater and healthy, black band diseased, and dead coral surfaces. *Applied and Environmental Microbiology*, v. 68, no. 5, p. 2214–2228. doi:10.1128/aem.68.5.2214-2228.2002

Fukami, H., Budd, A.F., Levitan, D.R., Jara, J., Kersanach, R., & Knowlton, N. (2004). Geographic differences in species boundaries among members of the Montastraea annularis complex based on molecular and morphological markers. *Evolution*, v. 58, no. 2, p. 324–337. doi:10.1111/j.0014-3820.2004.tb01648.x

Goreau, T.F. (1963). Calcium carbonate deposition by coralline algae and corals in relation to their roles as reef-builders. *New York Academy of Science*, v. 109, no. 1, p. 127-167. doi:10.1111/j.1749-6632.1963.tb13465.x

Haeckel, E. (1873). Kunstformen der Natur (Art Forms in Nature). Republished by *Pretsel Publishing*, 2018.

Hendy, E.J., Gagan, M.K., Lough, J.M., McCulloch, M., & deMenocal, P.B. (2007). Impact of skeletal dissolution and secondary aragonite on trace element and isotopic climate proxies in Porites corals. *Paleoceanography*, v. 22, no. 4, PA4101. doi:10.1029/2007pa001462

Hoegh-Guldberg, O., Mumby, P.J., Hooten, A.J., Steneck, R.S., Greenfield, P., Gomez, E., Harvell, C.D., Sale, P.F., Edwards, A.J., Caldiera, K., Knowlton, N., Eakin, C.M., Iglesias-Prieto, R., Muthiga, N., Bradbury, R.H., Dubi, A., & Hatziolos, M.E. (2007). Coral reefs under rapid climate change and ocean acidification. *Science*, v. 318, no. 5857, p. 1737–1742. doi:10.1126/science.1152509

Humann, P., and DeLoach, N. (2001). Reef coral identification: Florida, Caribbean, Bahamas (Reef Set, Vol. 3), 2nd Ed. *New World Publications Inc.* ISBN: 978-1878348326

IPCC (2018). Global warming of 1.5 degree C. http://www.ipcc.ch/report/sr15/.

Kitano, Y.F., Benzoni, F., Arrigoni, R., Shirayama, Y., Wallace, C.C., & Fukami, H. (2014). A phylogeny of the family Poritidae (Cnidaria, Scleractinia) based on molecular and morphological analyses. *PLoS ONE*, v. 9, no. 5, e98406. doi:10.1371/journal.pone.0098406

Klaus, J.S., Janse, I., Heikoop, J.M., Sanford, R.A., & Fouke, B.W. (2007). Coral microbial communities, zooxanthellae and mucus along gradients of seawater depth and coastal pollution. *Environmental Microbiology*, v. 9, no. 5, p. 1291–1305. doi:10.1111/j.1462-2920.2007.01249.x

Knowlton, N., Weil, E., Weigt, L.A., & Guzman, H.M. (1992). Sibling species in Montastraea annularis, coral bleaching, and the coral climate record. *Science*, v. 255, no. 5042, p. 330–333. doi: 10.1126/science.255.5042.330

Knowlton, N., & Budd, A.F. (2001). Recognizing coral species present and past. *Evolutionary Patterns. Growth Form, and Tempo in the Fossil Record*, 103-119.

Krawczyk, H., Zinke, J., Browne, N., Struck, U., McIlwain, J., O'Leary, M., & Garbe-Schönberg, D. (2020). Corals reveal ENSO-driven synchrony of climate impacts on both terrestrial and marine ecosystems in northern Borneo. *Scientific Reports*, v. 10, no. 3678. doi:10.1038/s41598-020-60525-1

Langmuir, C.H., Vocke, R.D., Hanson, G.N., & Hart, S.R. (1978). A general mixing equation with applications to Icelandic basalts. *Earth and Planetary Science Letters*, v. 37, no. 3, p. 380–392. doi:10.1016/0012-821x(78)90053-5

Lough, J.M., & Barnes, D.J. (1989). Possible relationships between environmental variables and skeletal density in a coral colony from the central Great Barrier Reef. *Journal of Experimental Marine Biology and Ecology*, v. 134, no. 3, p. 221–241. doi:10.1016/0022-0981(89)90071-3

Love, K.M., & Woronow, A. (1991). Chemical changes induced in aragonite using treatments for the destruction of organic material. *Chemical Geology*, v. 93, no. 3-4, p. 291–301. doi:10.1016/0009-2541(91)90119-c

McGregor, H.V., & Abram, N.J. (2008). Images of diagenetic textures in Porites corals from Papua New Guinea and Indonesia. *Geochemistry, Geophysics, Geosystems*, v. 9, no. 10, Q10013. doi:10.1029/2008gc002093

NOAA-NCDC (2020). https://coralreefwatch.noaa.gov/satellite/index.php.

Nothdurft, L.D., & Webb, G.E. (2007). Microstructure of common reef-building coral genera Acropora, Pocillopora, Goniastrea and Porites: constraints on spatial resolution in geochemical sampling. *Facies*, v. 53, no. 1, p. 1–26. doi:10.1007/s10347-006-0090-0

Ogilvie, M.M. (1896). Microscopic and systematic study of madreporarian types of corals. *Philosophical Transactions of the Royal Society B: Biological Sciences*, v. 187, p. 83–345. doi:10.1098/rstb.1896.0003

Quinn, T.M., & Taylor, F.W. (2006). SST artifacts in coral proxy records produced by early marine diagenesis in a modern coral from Rabaul, Papua New Guinea. *Geophysical Research Letters*, v. 33, no. 4, L04601. doi:10.1029/2005gl024972

Ricci, F., Rossetto Marcelino, V., Blackall, L.L., Kühl, M., Medina, M., & Verbruggen, H. (2019). Beneath the surface: community assembly and functions of the coral skeleton microbiome. *Microbiome*, v. 7, no. 1. doi:10.1186/s40168-019-0762-y

Rohwer, F., Seguritan, V., Azam, F., & Knowlton, N. (2002). Diversity and distribution of coral-associated bacteria. *Marine Ecology Progress Series*, v. 243, p. 1–10. doi: 10.3354/meps243001

Rowan, R. (2004). Thermal adaptation in reef coral symbionts. *Nature*, v. 430, no. 7001, p. 742–742. doi:10.1038/430742a

Salih, A., Larkum, A., Cox, G., Kühl, M., & Hoegh-Guldberg, O. (2000). Fluorescent pigments in corals are photoprotective. *Nature*, v. 408, no. 6814, p. 850–853. doi:10.1038/35048564

Sayani, H.R., Cobb, K.M., Cohen, A.L., Elliott, W.C., Nurhati, I.S., Dunbar, R.B., Rose, K.A., & Zaunbrecher, L.K. (2011). Effects of diagenesis on paleoclimate reconstructions from modern and young fossil corals. *Geochimica et Cosmochimica Acta*, v. 75, no. 21, p. 6361–6373. doi:10.1016/j.gca.2011.08.026

Schwarz, J.A., Brokstein, P.B., Voolstra, C.R., Terry, A.Y., Miller, D.J., Szmant, A.M., Coffroth, M.A., & Medina, M. (2008). Coral life history and symbiosis: functional genomic resources for two reef building Caribbean corals, Acropora palmata and Montastraea faveolata. *BMC Genomics*, v. 9, no. 1, p. 97. doi:10.1186/1471-2164-9-97

Sivaguru, M., Fried, G.A., Miller, C.H., & Fouke, B.W (2014). Multimodal optical microscopy methods reveal polyp tissue morphology and structure in Caribbean reef building corals. *Journal of Visualized Experiments*, v. 91, e51824.

Sivaguru, M., Fouke, K.W., Todorov, L., Kingsford, M.J., Fouke, K.E., Trop, J.M., & Fouke, B.W. (2019). Correction factors for δ18O-derived global sea surface temperature reconstructions from diagenetically altered intervals of coral skeletal density banding. *Frontiers in Marine Science*, v. 6. doi:10.3389/fmars.2019.00306

Stolarski, J. & Roniewicz, E. (2001). Towards a new synthesis of evolutionary relationships and classification of Scleractinia. *Journal of Paleontology*, v. 75, no. 6, p. 1090-1108. doi:10.1666/0022-3360(2001)075<1090:tansoe>2.0.co;2

Van Duyl, F.C. (1985). Atlas of the living reefs of Curaçao and Bonaire (Netherlands Antilles). *Foundation for Scientific Research in Suri-nam and the Netherlands Antilles*, v. 117, p. 37. ISSN: 0300-5534

Van Oppen, M.J.H., & Blackall, L.L. (2019). Coral microbiome dynamics, functions and design in a changing world. *Nature Reviews Microbiology*. doi:10.1038/s41579-019-0223-4

Van Veghel, M.L.J., & Bosscher, H. (1995). Variation in linear growth and skeletal density within the polymorhic reef building coral *Monastraea annularis*. *Bulletin in Marine Science*, v. 56, p. 902-907.

Veron, J.E.N. (2000). Corals of the world. Volume 3. *Australian Institute of Marine Science*, pp. 1-490.

Weil, E., & Knowton, N. (1994). A multi-character analysis of the Caribbean coral Montastraea annularis (Ellis and Solander, 1786) and its two sibling species, M. faveolata (Ellis and Solander, 1786) and M. franksi (Gregory, 1895). *Bulletin of Marine Science*, v. 55, no. 1, p. 151–175.

Wells, J.W. (1954). Recent corals of the Marshall Islands; fossil corals from Eniwetok Atoll. *U.S.G.S. Professional Paper,* v. 260, no. 1, pp. 478.

Wilson, J.L. (1975). Carbonate Facies in Geologic History. *Springer-Verlag*, New York, pp. 472.

Wórum, F.P., Carricart-Ganivet, J.P., Benson, L., & Golicher, D. (2007). Simulation and observations of annual density banding in skeletons of Montastraea (Cnidaria: Scleractinia) growing under thermal stress associated with ocean warming. *Limnology and Oceanography*, v. 52, no. 5, p. 2317–2323. doi:10.4319/lo.2007.52.5.2317

Zinke, J., Reuning, L., Pfeiffer, M., Wassenburg, J.A., Hardman, E., Jhangeer-Khan, R., Davies, G.R., Ng, C. K. C., & Kroon, D. (2016). A sea surface temperature reconstruction for the southern Indian Ocean tradewind belt from corals in Rodrigues Island (19° S, 63° E). *Biogeosciences*, v. 13, no. 20, p. 5827–5847. doi:10.5194/bg-13-5827-2016